

# The effect of auxeticity on the vibration of conical sandwich shells with ring support under various boundary conditions



Maysam Alinia <sup>a</sup>, Reza Nopour <sup>a</sup>, Mohammad Mohammadi Aghdam <sup>a,\*</sup>, Reza Hedayati <sup>a,b</sup>

<sup>a</sup> Department of Mechanical Engineering, Amirkabir University of Technology (Tehran Polytechnic), Tehran, Iran

<sup>b</sup> Department of Aerospace Structures and Materials, Faculty of Aerospace Engineering, Delft University of Technology (TU Delft), Kluyverweg 1, 2629 HS, Delft, The Netherlands

## ARTICLE INFO

### Keywords:

Vibration  
Auxetic core  
GDQ method  
Conical shell  
Ring support

## ABSTRACT

Auxetic materials, materials demonstrating negative Poisson's ratio, have revolutionized the use of materials in industries, as they demonstrate superb acoustic response, fracture resistance, and energy absorption. For the first time, this study embraces the free vibration of conical shells consisting of an auxetic core with and without ring support under various boundary conditions. First, the material characteristics of the auxetic core are calculated by means of a micromechanical approach. Afterwards, the kinematic motion equations of the conical shell are derived utilizing the first-order shear deformation theory. Finally, the governing equations are solved using the powerful generalized differential quadrature element method (GDQEM). The primary goal of this paper is to study the role of implementing an auxetic core as well as ring support in determining the vibrational behavior of the structure. The results of the study showed that the honeycomb interior angle and the presence of ring support can significantly affect the natural frequency of the structure. Lower frequencies can be reached as the interior angle increases. The importance of ring position is found to be highly dependent on the longitudinal mode shapes of vibration. The impact of ring position on natural frequencies is affected by the semi-vertex angle of the cone, and a shift in frequency peaks can be observed by increasing the semi-vertex angle.

## 1. Introduction

The value of Poisson's ratio plays a vital role in industrial products. Biomedical implants, aircraft parts [1], energy production facilities, and sports equipment are examples of applications where every element deformation needs to be addressed carefully. With exponential growth in manufacturing technologies, the application of new types of artificial materials, such as metamaterials, is increasing rapidly. Auxetics are an important type of metamaterials which, unlike conventional materials, show a negative Poisson's ratio. In other words, the auxetic meta-materials do not shrink laterally under the uniaxial extension, but they show expansion [1]. This has led to some interesting mechanical and physical properties, such as superb acoustic response, improved energy absorption capability, and enhanced shear modulus and fracture toughness [2].

Employing a theoretical scheme, Dirrenberger et al. [3] studied the effective elastic characteristics of anisotropic three auxetic microstructures. In another comprehensive research, an idealized 3D re-entrant auxetic structure was studied analytically, numerically, and

experimentally [4]. They implemented Euler-Bernoulli and Timoshenko beam theories for their analytical study. Auxetic meta-biomaterials have been studied in terms of mechanical and fatigue performances as they can potentially improve implant-bone biological and physical interaction [4–8]. In another experimental work, Plewa et al. [9] analyzed planar and tubular auxetic patterns fabricated by the additive manufacturing (AM) technique. Through a discrete homogenization scheme, the properties of composite materials made of auxetic inclusions (hexachiral and hexagonal reentrant lattices) were studied by Assidi and Ganghoffer [10]. Kochmann and Venturini [11] implemented structural elements with rotational degrees of freedom as a design principle for finitely strained composites made of stiff inclusions in a hyperelastic matrix. Furthermore, auxetic structures show excellent energy absorption [12] and impact resistance performance [13]. In another work, Nedoushan et al. [14] presented a fully triangular architecture based on anti-tetra chiral configuration to enhance structural stiffness. Jiang et al. [15] investigated the effect of using multilayer orthogonal auxetic reinforcement in polyurethane foam matrix on the failure of composite panels, demonstrating extraordinary damping and

\* Corresponding author.

E-mail address: [aghdam@aut.ac.ir](mailto:aghdam@aut.ac.ir) (M.M. Aghdam).

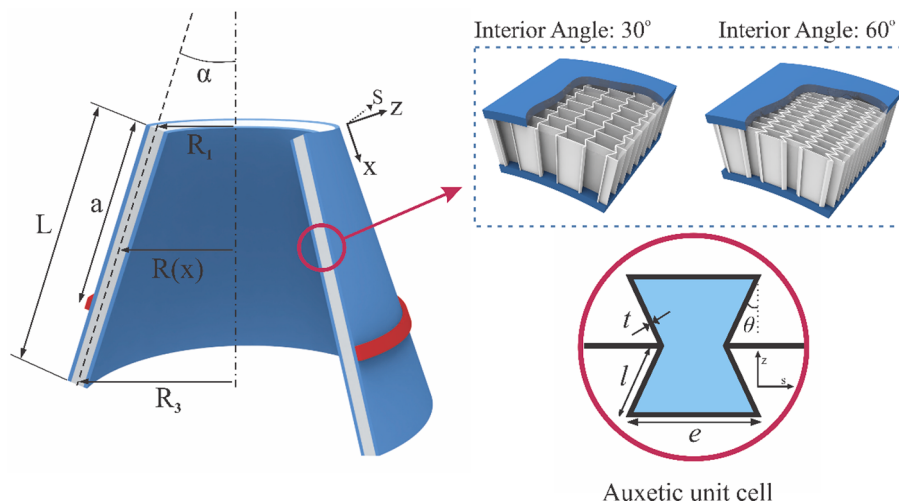


Fig. 1. The geometry and dimensions of a conical shell with an auxetic core. The extreme cases of  $\theta = 30^\circ$  and  $\theta = 60^\circ$  are demonstrated visually.

large range of deformation performance. Li et al. [16] combined auxetic materials as a reinforcing agent inside incompressible soft elements to create composites with enhanced indentation stiffness and impact resistance.

As mentioned above, auxetic structures are unique patterns to be used in many industrial applications. Many researchers, therefore, have studied the dynamic and static characteristics of multi-layered laminated composite panels made of or combined with auxetic components. For example, vibration and nonlinear dynamic response of sandwich panels with auxetic core were studied by Duc et al. [17]. In terms of auxetic plates, Lim investigated the vibrations and buckling behaviors of circular auxetic plates [18]. Nonlinear chaotic oscillations of composite beams with auxetic carbon nanotube reinforcement were studied by Parhi et al. [19]. The effect of auxeticity on energy absorption and low-velocity impact behavior of sandwich structures was investigated by Jiang and Hu in an experimental work [20]. The post-buckling behavior of an auxetic beam was studied by Dabbagh and Ebrahimi [21], and showed that utilizing small auxeticity angles results in more strengthened buckling characteristics. Moreover, the effect of auxetic layers' thicknesses on the deflection of a laminated composite with an auxetic ply was investigated by Ebrahimi et al. [22]. Similarly, Hajmohammad et al. [23] surveyed face sheets with auxetic core blast characteristics, which improved the dynamic behavior. Recently, with the help of Differential Quadrature Method (DQM), Behravan Rad [24] studied the effect of auxetic structures on the static bending of functionally graded circular plates. Regarding the nonlinear dynamic characteristics of sandwich beams, Li et al. [25] reported that auxetic parameters can significantly influence the dynamic response of the structure. Furthermore, they analyzed their proposed model, 3D double-V meta-lattice core and FG GRC facesheets, in case of low-velocity impact [26]. Further studies regarding dynamic behaviors of auxetic material with a with negative Poisson's ratio can be found in literature [27–30].

Speaking of DQM, many efforts have been made toward analyzing composite laminates or sandwich panels using the Generalized Differential Quadrature (GDQ) and similar methods. For example, Tornabene et al. [31] analyzed damaged configurations and static behavior of composite structures using the GDQ method. In another research, the generalized differential quadrature element method (GDQEM) was used to estimate the frequencies of a plate reinforced with graphene platelets [32]. Moreover, Bagheri et al. used GDQ to evaluate the free vibration behavior of a joined conical–cylindrical–conical shell structure [33]. More studies concerning the DQM technique in composite structures can be found in Refs. [34–41]. The presence of a ring in a shell is also an interesting topic of research, which has a beneficial impact on vibration characteristics and frequency response of the system [42]. Hou et al.

[43], therefore, examined the free vibration of a conical shell consisting of an intermediate ring support utilizing GDQEM. Similarly, using the First-order Shear Deformation Theory (FSDT), the free vibration of an isotropic homogeneous shell containing a middle ring was analyzed with the help of GDQ by Bagheri et al. [44]. Furthermore, Dong et al. [45], using a support ring as a controller, studied the free vibration behavior of a conical shell. Their study used a modified version of GDQEM which was combined with trigonometric expansion (TE) analysis.

Looking at the previous works, it can be seen that the effect of the middle ring on isotropic shells is studied [44]; moreover, the analysis of auxetic honeycomb core in panels and truncated conical sandwich shells have also been conducted in [46–48]. Furthermore, various solution methods such as Galerkin, GDQ and Rayleigh-Ritz can be found excessively in the investigations [49–52]. To the best of the author's knowledge, an analytical study on the effect of auxeticity on the vibration behavior of conical shells with (and without) ring support is lacking in the literature. Due to the presence of this deficiency in the studies and the importance of conical shells as an essential part of aircraft, offshore, and tubular structures [53], the present manuscript studies the free vibration of conical sandwich panels with auxetic cores utilizing powerful GDQEM.

To this aim, first and foremost, the material properties of the auxetic ply are found through a micromechanical technique. Next, employing the first-order theory of shells, the governing equations are obtained for a conical sandwich shell. Later, two sets of governing equations, one for the lower segment and one for the upper segment (i.e. elements) of the cone, are considered, and the boundary conditions imposed by the ring as well as the continuity condition at that region, are taken into account. Finally, the GDQEM is employed to solve the system of equations related to the eigenvalue problem. The solution is performed for various combinations of simply supported (S) and clamped (C) boundary conditions. Parametric studies are performed to evaluate the effect of the main cone angle as well as the unit cell internal angle on the natural frequency of the cone.

## 2. Methodology

### 2.1. Shell structure description

A three-layered sandwich conical shell stiffened with an intermediate ring, including two skin layers made of isotropic material and the core layer made of re-entrant auxetic metamaterial with a negative Poisson's ratio, was considered for this study. The geometry described above is schematically depicted in Fig. 1. The origin of the coordinate system ( $x, s, z$ ) is set to be at the highest point of the mid-plane of the

core of the sandwich panel. The range of change of the variables was hence  $0 \leq x \leq L$ ,  $0 \leq s \leq 2\pi$ , and  $-h/2 \leq z \leq h/2$ . The conical shell structure was reinforced by the ring support at  $x = a$ . The parameters  $R_1$ ,  $R_2$ , and  $R_3$  denote the radii of the smallest section, the ring section, and the largest section of the cone.

## 2.2. Core material characteristics

First and foremost, it is important to have analytical relationships for the mechanical properties of the auxetic core in terms of its micro-structural dimensions shown in Fig. 1. The effective material properties of the considered re-entrant auxetic structure are as follows [54]:

$$\begin{aligned} E_1^{(c)} &= E \frac{\kappa^3(\lambda - \sin\theta)}{\cos\theta[1 + (\tan^2\theta + \lambda\sec^2\theta)\kappa^2]}, \\ E_2^{(c)} &= E \frac{\kappa^3}{\cos\theta(\tan^2\theta + \kappa^2)(\lambda - \sin\theta)}, \\ G_{12}^{(c)} &= G \frac{\kappa^3}{\lambda_1(1 + 2\lambda)\cos\theta}, \\ G_{23}^{(c)} &= G \frac{\kappa\cos\theta}{\lambda - \sin\theta}, \\ G_{13}^{(c)} &= G \frac{\kappa^3}{2\cos\theta} \left[ \frac{\lambda - \sin\theta}{1 + 2\lambda} + \frac{\lambda + 2\sin^2\theta}{2(\lambda - \sin\theta)} \right], \\ \nu_{12}^{(c)} &= -\frac{\sin\theta(1 - \kappa^2)(\lambda - \sin\theta)}{\cos^2\theta[1 + (\tan^2\theta + \sec^2\theta\lambda)\kappa^2]}, \quad \nu_{21}^{(c)} = \frac{-\sin\theta(1 - \kappa^2)}{(\tan^2\theta + \kappa^2)(\lambda - \sin\theta)}, \\ \rho^c &= \rho \frac{\kappa(\lambda + 2)}{2\cos\theta(\lambda - \sin\theta)} \end{aligned} \quad (1)$$

where  $\lambda = e/l$  and  $\kappa = t/l$ . The subscript "c" represents the properties related to the core layer. In the above equations,  $t$  denotes the thickness of the cell walls, and  $e$  and  $l$  stand for horizontal and inclined cell wall lengths, respectively. Moreover,  $E$ ,  $G$ , and  $\rho$  represent Young's modulus, shear modulus, and density of the material that the auxetic core is made of, respectively. It is worth mentioning that the resulting properties achieved from the above definitions can have uncertainties due to the possibility of the presence of uncertainty in the value of the input parameters. In the present study, the ideal situation with no uncertainty in input variables has been considered. Having said that, the readers interested in uncertainty analysis are referred to [55–58].

## 2.3. The governing equations

The FSDT theory is employed for each truncated cone element (i.e. segment) to formulate the governing equations of the conical sandwich shell. The subscript  $i = 1, 2$  refer to each element (i.e. segment) of the conical shell. Accordingly, the displacement field of a generic point in the shell structure can be written as [44,59]:

$$\begin{aligned} u^i(x, s, z, t) &= u_0^i(x, s, t) + z\varphi_x^i(x, s, t) \\ v^i(x, s, z, t) &= v_0^i(x, s, t) + z\varphi_s^i(x, s, t) \\ w^i(x, s, z, t) &= w_0^i(x, s, t) \end{aligned} \quad (2)$$

where the displacement components in the axial  $x$ , circumferential  $s$ , and radial  $z$  directions are denoted by  $u$ ,  $v$ , and  $w$ , respectively.  $\varphi_x$  and  $\varphi_s$  stand for normal transverse rotation about  $s$  and  $x$ . The strain field on any point of the sandwich conical shell can be written as

$$\begin{Bmatrix} \epsilon_{xx}^i \\ \epsilon_{ss}^i \\ \gamma_{xs}^i \\ \gamma_{xz}^i \\ \gamma_{sz}^i \end{Bmatrix} = \begin{Bmatrix} \epsilon_{xx0}^i \\ \epsilon_{ss0}^i \\ \gamma_{xs0}^i \\ \gamma_{xz0}^i \\ \gamma_{sz0}^i \end{Bmatrix} + z \begin{Bmatrix} \kappa_{xx}^i \\ \kappa_{ss}^i \\ \kappa_{xz}^i \\ \kappa_{sz}^i \end{Bmatrix} \quad (3)$$

where the strain components and curvature changes are defined by:

$$\begin{Bmatrix} \epsilon_{xx0}^i \\ \epsilon_{ss0}^i \\ \gamma_{xs0}^i \\ \gamma_{xz0}^i \\ \gamma_{sz0}^i \end{Bmatrix} = \begin{Bmatrix} u_{0,x}^i \\ \frac{v_{0,s}^i}{R} + \frac{u_{0,s}^i}{R}\sin(\alpha) + \frac{w_{0,s}^i}{R}\cos(\alpha) \\ v_{0,x}^i + \frac{u_{0,s}^i}{R} - \frac{v_{0,s}^i}{R}\sin(\alpha) \\ w_{0,x}^i + \varphi_x^i \\ \frac{w_{0,s}^i}{R} - \frac{v_{0,s}^i}{R}\cos(\alpha) + \varphi_s^i \end{Bmatrix} \quad (4)$$

and

$$\begin{Bmatrix} \kappa_{xx}^i \\ \kappa_{ss}^i \\ \kappa_{xs}^i \\ \kappa_{xz}^i \\ \kappa_{sz}^i \end{Bmatrix} = \begin{Bmatrix} \varphi_{x,x}^i \\ \frac{\varphi_{s,s}^i}{R} + \frac{\varphi_x^i}{R}\sin(\alpha) \\ \frac{\varphi_{x,s}^i}{R} + \varphi_{s,x}^i - \frac{\varphi_s^i}{R}\sin(\alpha) \\ 0 \\ 0 \end{Bmatrix} \quad (5)$$

in which, derivative with respect to  $x$  and  $s$  are shown with subscript ' $x$ ' and ' $s$ ', respectively. where  $\alpha$  denotes the semi-vertex angle of the cone. By assuming the case of linear elasticity, the stress resultants can be derived as

$$\begin{aligned} \begin{bmatrix} N_x^i \\ N_s^i \\ N_{xs}^i \\ M_x^i \\ M_s^i \\ M_{xs}^i \end{bmatrix} &= \begin{bmatrix} A_{11} & A_{12} & A_{16} & B_{11} & B_{12} & B_{16} \\ A_{12} & A_{22} & A_{26} & B_{12} & B_{22} & B_{26} \\ A_{16} & A_{26} & A_{66} & B_{16} & B_{26} & B_{26} \\ B_{11} & B_{12} & B_{16} & D_{11} & D_{12} & D_{16} \\ B_{12} & B_{22} & B_{26} & D_{12} & D_{22} & D_{26} \\ B_{16} & B_{26} & B_{66} & D_{16} & D_{26} & D_{66} \end{bmatrix} \begin{bmatrix} \epsilon_{xx0}^i \\ \epsilon_{ss0}^i \\ \gamma_{xs0}^i \\ \kappa_{xx}^i \\ \kappa_{ss}^i \\ \kappa_{xs}^i \end{bmatrix} \\ \begin{bmatrix} Q_s^i \\ Q_x^i \end{bmatrix} &= k_C \begin{bmatrix} A_{44} & A_{45} \\ A_{45} & A_{55} \end{bmatrix} \begin{bmatrix} \gamma_{sz}^i \\ \gamma_{xz}^i \end{bmatrix} \end{aligned} \quad (6)$$

where  $k_C$  represents the transverse shear correction factor that results in a more accurate estimation of the solution. In this study,  $k_C$  is assumed to be  $5/6$  [60–62]. The coefficients  $A_{ij}$ ,  $B_{ij}$ , and  $D_{ij}$  are the components of the extensional, coupling, and bending stiffness matrices of the conical sandwich shell, respectively. In other words:

$$\begin{aligned} (A_{ij}, B_{ij}, D_{ij}) &= \int_{-h/2}^{-hc/2} Q_{ij}(1, z, z^2) dz + \int_{-hc/2}^{hc/2} Q_{ij}^C(1, z, z^2) dz \\ &\quad + \int_{hc/2}^{h/2} Q_{ij}(1, z, z^2) dz \end{aligned} \quad (7)$$

where  $h_c$  stands for the core thickness. Moreover, the stiffness coefficients of the auxetic core and isotropic skin layers can be written as follows

$$\begin{aligned} Q_{11}^C &= \frac{E_1^C}{1 - v_{12}^C v_{21}^C}, Q_{12}^C = \frac{v_{12}^C E_2^C}{1 - v_{12}^C v_{21}^C}, \\ Q_{22}^C &= \frac{E_2^C}{1 - v_{12}^C v_{21}^C}, Q_{44}^C = G_{23}^C, Q_{55}^C = Q_{66}^C = G_{12}^C, \\ Q_{11} &= \frac{E}{1 - v^2}, Q_{12} = \frac{vE}{1 - v^2}, Q_{22} = Q_{11} \\ Q_{44} &= Q_{55} = Q_{66} = \frac{E}{2(1 + v)} \end{aligned} \quad (8)$$

where  $v$  stands for Poisson's ratio. Lastly, utilizing Hamilton's principle, the equations of motion of the conical sandwich shell can be found as [59]:

$$\begin{aligned} N_{x,x}^i + \frac{1}{R} N_{xs,s}^i + (N_x^i - N_s^i) \frac{\sin(\alpha)}{R} &= I_0 \ddot{u}_0^i + I_1 \ddot{\varphi}_x^i \\ N_{xs,s}^i + \frac{1}{R} N_{s,s}^i + Q_s^i \frac{\cos(\alpha)}{R} + 2N_{xs}^i \frac{\sin(\alpha)}{R} &= I_0 \ddot{v}_0^i + I_1 \ddot{\varphi}_s^i \\ Q_{x,x}^i + \frac{1}{R} Q_{xs,s}^i + Q_x^i \frac{\sin(\alpha)}{R} + N_s^i \frac{\cos(\alpha)}{R} &= I_0 \ddot{w}_0^i \\ M_{x,x}^i + \frac{1}{R} M_{xs,s}^i + (M_x^i - M_s^i) \frac{\sin(\alpha)}{R} - Q_x &= I_1 \ddot{u}_0^i + I_2 \ddot{\varphi}_x^i \\ M_{xs,s}^i + \frac{1}{R} M_{s,s}^i + 2M_{xs}^i \frac{\sin(\alpha)}{R} - Q_s &= I_0 \ddot{v}_0^i + I_1 \ddot{\varphi}_s^i \end{aligned} \quad (9)$$

where  $I_0$ ,  $I_1$ , and  $I_2$  are the mass moments of inertia, which are defined as

$$(I_0, I_1, I_2) = \int_{-h/2}^{-h_c/2} \rho(1, z, z^2) dz + \int_{-h_c/2}^{h_c/2} \rho^c(1, z, z^2) dz + \int_{h_c/2}^{h/2} \rho(1, z, z^2) dz \quad (10)$$

The parameter  $R$  represents the radius of any point on the shell along the axial direction for each cone element  $i = 1, 2$  and is equal to:

$$R = R_i + x \sin(\alpha) \quad (11)$$

Employing the separation of variables technique in correlation with Fourier series expansion according to [63,64], the displacement and rotation components can be written as:

$$\begin{aligned} u_0^i(x, s, t) &= U^i(x) \cos(ns) e^{i\omega t} \\ v_0^i(x, s, t) &= V^i(x) \sin(ns) e^{i\omega t} \\ w_0^i(x, s, t) &= W^i(x) \cos(ns) e^{i\omega t} \\ \varphi_x^i(x, s, t) &= \Phi_x^i(x) \cos(ns) e^{i\omega t} \\ \varphi_s^i(x, s, t) &= \Phi_s^i(x) \sin(ns) e^{i\omega t} \end{aligned} \quad (12)$$

where  $U$ ,  $V$ ,  $W$ ,  $\Phi_x$  and  $\Phi_s$  are unknown functions.  $n$  denotes the circumferential wave number of the associated mode shape, and  $\omega$  is the natural frequency. By substituting Eq. (6) into Eq. (9), and utilizing Eq. (12) to separate variables, and then by integrating through circumferential direction from 0 to  $2\pi$ , the two-dimensional problem ( $x, s$ ) is reduced to a one-dimensional problem, and the variable  $s$  can be eliminated. The governing equations can, therefore, be expressed as [59]:

$$\begin{aligned} \Psi_{111} U + \Psi_{112} U_{,x} + \Psi_{113} U_{,xx} + \Psi_{121} V + \Psi_{122} V_{,x} + \Psi_{131} W + \Psi_{132} W_{,x} + \Psi_{141} \Phi_x + \\ \Psi_{142} \Phi_{x,x} + \Psi_{143} \Phi_{x,xx} + \Psi_{151} \Phi_s + \Psi_{152} \Phi_{s,x} + I_0 \omega^2 R^2 U + I_1 \omega^2 R^2 \Phi_x = 0, \\ \Psi_{211} U + \Psi_{212} U_{,x} + \Psi_{221} V + \Psi_{222} V_{,x} + \Psi_{223} V_{,xx} + \Psi_{231} W + \Psi_{241} \Phi_x + \\ \Psi_{242} \Phi_{x,x} + \Psi_{251} \Phi_s + \Psi_{252} \Phi_{s,x} + \Psi_{253} \Phi_{s,xx} + I_0 \omega^2 R^2 V + I_1 \omega^2 R^2 \Phi_s = 0, \\ \Psi_{311} U + \Psi_{312} U_{,x} + \Psi_{321} V + \Psi_{322} V_{,x} + \Psi_{323} W + \Psi_{341} \Phi_x + \Psi_{332} W_{,x} + \Psi_{333} W_{,xx} + \Psi_{341} \Phi_x + \\ \Psi_{342} \Phi_{x,x} + \Psi_{351} \Phi_s + I_0 \omega^2 R^2 W = 0, \\ \Psi_{411} U + \Psi_{412} U_{,x} + \Psi_{413} U_{,xx} + \Psi_{421} V + \Psi_{422} V_{,x} + \Psi_{431} W + \Psi_{432} W_{,x} + \Psi_{441} \Phi_x + \\ \Psi_{442} \Phi_{x,x} + \Psi_{443} \Phi_{x,xx} + \Psi_{451} \Phi_s + \Psi_{452} \Phi_{s,x} + I_1 \omega^2 R^2 U + I_2 \omega^2 R^2 \Phi_x = 0, \\ \Psi_{511} U + \Psi_{512} U_{,x} + \Psi_{521} V + \Psi_{522} V_{,x} + \Psi_{523} V_{,xx} + \Psi_{531} W + \Psi_{541} \Phi_x + \\ \Psi_{542} \Phi_{x,x} + \Psi_{551} \Phi_s + \Psi_{552} \Phi_{s,x} + \Psi_{553} \Phi_{s,xx} + I_1 \omega^2 R^2 V + I_2 \omega^2 R^2 \Phi_s = 0. \end{aligned} \quad (13)$$

where  $\Psi$  can be written as [59]:

$$\begin{aligned} \Psi_{111} &= -A_{66} n^2 - A_{22} \sin^2 \alpha, \Psi_{112} = A_{11} R \sin \alpha \\ \Psi_{113} &= A_{11} R^2, \Psi_{121} = -A_{66} n \sin \alpha - A_{22} n \sin \alpha \\ \Psi_{122} &= (A_{12} + A_{66}) n R, \Psi_{131} = -A_{22} \sin \alpha \cos \alpha, \Psi_{132} = A_{12} R \cos \alpha \\ \Psi_{141} &= -B_{66} n^2 - B_{22} \sin^2 \alpha, \Psi_{142} = B_{11} R \sin \alpha, \Psi_{143} = B_{11} R^2 \\ \Psi_{151} &= -B_{66} n \sin \alpha - B_{22} n \sin \alpha, \Psi_{152} = (B_{12} + B_{66}) n R \\ \Psi_{211} &= -A_{66} n \sin \alpha - A_{22} n \sin \alpha, \Psi_{212} = -(A_{12} + A_{66}) n R \\ \Psi_{221} &= -A_{22} n^2 - A_{66} \sin^2 \alpha - k_c A_{44} \cos^2 \alpha \\ \Psi_{222} &= A_{66} R \sin \alpha, \Psi_{231} = -A_{22} n \cos \alpha - k_c A_{44} n \cos \alpha \\ \Psi_{241} &= -B_{22} n \sin \alpha - B_{66} n \sin \alpha, \Psi_{242} = -(B_{12} + B_{66}) n R \\ \Psi_{251} &= -B_{22} n^2 - B_{66} \sin^2 \alpha + k_c A_{44} R \cos \alpha \\ \Psi_{252} &= B_{66} R \sin \alpha, \Psi_{253} = B_{66} R^2, \Psi_{311} = -A_{22} \cos \alpha \sin \alpha \\ \Psi_{312} &= -A_{12} R \cos \alpha, \Psi_{321} = -A_{22} n \cos \alpha - k_c A_{44} n \cos \alpha \\ \Psi_{331} &= -k_c A_{44} n^2 - A_{22} \cos^2 \alpha, \Psi_{332} = k_c A_{55} R \sin \alpha \\ \Psi_{333} &= k_c A_{55} R^2, \Psi_{341} = k_c A_{55} R \sin \alpha - B_{22} \cos \alpha \sin \alpha \\ \Psi_{342} &= -B_{12} R \cos \alpha + k_c A_{55} R^2, \Psi_{351} = k_c A_{44} n R - B_{22} n \cos \alpha \\ \Psi_{411} &= -B_{66} n^2 - B_{22} \sin^2 \alpha, \Psi_{412} = B_{11} R \sin \alpha \\ \Psi_{413} &= B_{11} R^2, \Psi_{421} = -B_{66} n \sin \alpha - B_{22} n \sin \alpha \\ \Psi_{422} &= (B_{12} + B_{66}) n R, \Psi_{431} = -B_{22} \cos \alpha \sin \alpha \\ \Psi_{432} &= -k_c A_{55} R^2 - B_{12} R \cos \alpha, \Psi_{441} = -D_{66} n^2 - D_{22} \sin^2 \alpha - k_c A_{55} R^2 \\ \Psi_{442} &= D_{11} R \sin \alpha, \Psi_{443} = D_{11} R^2 \\ \Psi_{451} &= -D_{66} n \sin \alpha - D_{22} n \sin \alpha, \Psi_{452} = (D_{12} + D_{66}) n R \\ \Psi_{511} &= -B_{22} n \sin \alpha - B_{66} n \sin \alpha, \Psi_{512} = -(B_{12} + B_{66}) n R \\ \Psi_{521} &= -B_{22} n^2 + k_c A_{44} R \cos \alpha - B_{66} \sin^2 \alpha, \Psi_{522} = B_{66} R \sin \alpha \\ \Psi_{523} &= B_{66} R^2, \Psi_{531} = -B_{22} n \cos \alpha + k_c A_{44} n R \\ \Psi_{541} &= -D_{22} n \cos \alpha - D_{66} n \sin \alpha, \Psi_{542} = -(D_{12} + D_{66}) n R \\ \Psi_{551} &= -D_{22} n^2 - D_{66} \sin^2 \alpha - k_c A_{44} R^2, \Psi_{552} = D_{66} R \sin \alpha \\ \Psi_{553} &= D_{66} R^2 \end{aligned} \quad (14)$$

#### 2.4. Continuity and boundary conditions

Due to the presence of the ring and hence the implementation of two sets of governing equations, the continuity conditions of displacements and stresses need to be met at the interface of two cone elements. The essential continuity conditions are [44]:

$$\begin{aligned} w_0^1 &= 0, w_0^2 = 0, \\ u_0^1 &= u_0^2, v_0^1 = v_0^2, \\ \varphi_x^1 &= \varphi_x^2, \varphi_s^1 = \varphi_s^2 \end{aligned} \quad (15)$$

Moreover, the natural continuity conditions must be satisfied similarly as

$$\begin{aligned} N_{xx}^1 &= N_{xx}^2, M_{xx}^1 = M_{xx}^2, \\ N_{xs,s}^1 &= N_{xs,s}^2, M_{xs,s}^1 = M_{xs,s}^2 \end{aligned} \quad (16)$$

This study exploits two types of boundary conditions: clamped (C) and simply supported (S). The constraints used for each type of boundary condition on the edges of the conical sandwich shell are as follows:

$$\begin{aligned} C: u_0 &= v_0 = w_0 = \varphi_x = \varphi_s = 0 \\ S: u_0 &= v_0 = w_0 = M_x = \varphi_s = 0 \end{aligned} \quad (17)$$

**Table 1**

Comparison of dimensionless frequency  $\Omega = \omega R_1 \sqrt{\rho h / A_{11}}$  for the cross-ply conical shell ( $L = 2$  m,  $h = 0.01$  m,  $R = 1$  m,  $E_1 = 15$ ,  $E_2 = 10$  GPa,  $G_{12} = G_{13} = 0.6E_2$ ,  $G_{23} = 0.5E_2$ ,  $\nu_{12} = 0.25$ ,  $\rho = 1500 \frac{\text{kg}}{\text{m}^3}$ ,  $n = 1$ ).

	$\alpha$	[0/30/0]		[0/60/0]		[0/90/0]				
		Present	Xiang et al. [59]	Guo et al. [81]	Present	Xiang et al. [59]	Guo et al. [81]	Present	Xiang et al. [59]	Guo et al. [81]
C – C	90°	0.1474	0.1474	0.1556	0.1611	0.1611	0.1701	0.1633	0.1633	0.1723
	60°	0.1698	0.1698	0.1722	0.2128	0.2128	0.2126	0.2080	0.2081	0.2130
	30°	0.2264	0.2264	0.2186	0.3121	0.3121	0.3030	0.2682	0.2682	0.2706
	0°	0.2980	0.2980	0.2989	0.3837	0.3837	0.3850	0.2894	0.2894	0.2906
S – S	90°	0.0738	0.0738	0.0781	0.0808	0.0808	0.0856	0.0819	0.0819	0.0868
	60°	0.1110	0.1110	0.1048	0.1594	0.1594	0.1475	0.1550	0.1550	0.1500
	30°	0.1853	0.1853	0.1677	0.2785	0.2785	0.2579	0.2367	0.2367	0.2317
	0°	0.2707	0.2707	0.2712	0.3621	0.3621	0.3632	0.2650	0.2650	0.2661

## 2.5. Solution using the GDQE method

Various techniques are introduced in the open literature to solve numerous differential equations in Mechanical Engineering. Some approaches use approximation techniques by discretizing domain and boundary conditions to solve the problem [52,65–69], while more recently, due to the rapid development in neural network (NN) and machine learning, some methods such as deep neural network (DNN) [70–73], and Physics-Informed Neural Network (PINN), a DNN method integrated with the physical information of the problem, [74] have been presented for solving partial differential equations. A robust numerical procedure for solving differential equations, which is popular due to its fast convergence behavior and its precision, is the general differential quadrature (GDQ) method [75,76]. Having said that, it has its limitations in solving problems that include material and geometrical discontinuities in the computational domain, which can lead to singularities in eigenvalue problems. Therefore, GDQEM was introduced to have more flexibility in selecting the grid points and different boundary conditions [77,78]. If  $f$  is the solution to the differential equation, and  $C_{ij}^k$  are the weighting coefficients, the derivative of  $f(x)$  can be written as:

$$f_i^{(k)} = \sum_{j=1}^N C_{ij}^{(k)} f_j \quad (18)$$

where  $f_j$  stands for the value of  $f$  at discrete point  $x_j$ ,  $k$  represents the order of derivative, and  $N$  represents the number of grid points. Therefore, the weighing coefficients can be obtained as

$$C_{ij}^{(1)} = \begin{cases} \prod_{k=1, k \neq i, j}^N (x_i - x_k) / \prod_{k=1, k \neq j}^N (x_j - x_k) & (i \neq j) \\ \sum_{k=1, k \neq i}^N 1 / (x_i - x_k) & (i = j) \end{cases} \quad (19)$$

Equation (19) shows the weight coefficient matrix of the first derivatives. Weight coefficients for higher derivatives can be derived as:

$$C_{ij}^{(p)} = \sum_{k=1}^N C_{ik}^{(p-1)} C_{kj}^{(1)} \quad p = 2, 3, 4, \dots \quad (20)$$

Numerous techniques exist for the generation of grid distribution. In this study, Gauss–Chebyshev–Lobatto is chosen due to its high precision [79,80]. Using the GDQE technique, the problem domain in the axial direction is discretized into  $N$  nodal points. All differential equations, including the governing equations, the boundary conditions, and continuity constraints, are transformed into algebraic expressions using GDQEM coefficient matrices and can be written in matrix form.

Regarding the discontinuity of shell geometry induced by constraints due to the presence of a stiffened ring, stiffness and mass matrices for a one-dimensional problem with two elements can be written in a diagonal form as follows:

$$\begin{aligned} [K] &= \begin{bmatrix} [K^{(1)}] & [0] \\ [0] & [K^{(2)}] \end{bmatrix} \{q\} = \begin{bmatrix} \{q^{(1)}\} \\ \{q^{(2)}\} \end{bmatrix} [T] = \begin{bmatrix} [T_B] \\ [T_C] \end{bmatrix} \\ [M] &= \begin{bmatrix} [M^{(1)}] & [0] \\ [0] & [M^{(2)}] \end{bmatrix} \{q^{(i)}\} = \{U^i \ V^i \ W^i \ \Phi_X^i \ \Phi_S^i\} \end{aligned} \quad (21)$$

where stiffness  $[K]$  and mass  $[M]$  matrices are diagonal, and the displacement vector  $\{q\}$  contains the displacement components of all boundary and interface points. The matrix  $[T]$ , contains the equations derived for boundary and continuity conditions. Subscripts "B" and "C" in the above equations represent the boundary and continuity terms. At the cone top and bottom levels and interface nodes where the boundary and continuity equations are satisfied, the governing equations are ignored. This can be done by removing the associated rows in stiffness and mass matrices, and the equation can be obtained as follows:

$$[K]\{q\} = \omega^2 [M]\{q\} \quad (22)$$

By separating the displacement components of internal nodes from those of boundary and interface nodes, the matrices  $K$ ,  $M$ , and  $T$  can be modified and used in the governing equation as follows:

$$\begin{aligned} [\bar{K}_B]\{q_B\} + [\bar{K}_D]\{q_D\} &= \omega^2 ([\bar{M}_B]\{q_B\} + [\bar{M}_D]\{q_D\}), \\ [\bar{T}_B]\{q_B\} + [\bar{T}_D]\{q_D\} &= \{0\} \end{aligned} \quad (23)$$

Consequently, the algebraic system of equations in the form of an eigenvalue problem can be written as:

$$[K^*]\{q_D\} = \omega^2 [M^*]\{q_D\} \quad (24)$$

where the matrices  $[K^*]$  and  $[M^*]$  are defined as:

$$\begin{aligned} [K^*] &= [\bar{K}_D] + [\bar{K}_B] (- [\bar{T}_B]^{-1} [\bar{T}_D]), \\ [M^*] &= [\bar{M}_D] + [\bar{M}_B] (- [\bar{T}_B]^{-1} [\bar{T}_D]) \end{aligned} \quad (25)$$

Ultimately, by solving the eigenvalue problem presented in Eq. (24), the natural frequencies of the system can be found.

## 3. Results

### 3.1. Validation

The first frequency responses of the conical shells obtained from the proposed analytical method are compared with those available in the literature to evaluate the accuracy of the model. The

**Table 2**

Comparison of the dimensionless frequency of isotropic S-S cylinder ( $m = 1, E = 210 \text{ GPa}, \frac{R}{L} = 2, \frac{h}{R} = 0.06, \nu = 0.3, \rho = 7850 \frac{\text{kg}}{\text{m}^3}, \omega = \Omega \left( \frac{h}{\pi} \right) \sqrt{\frac{2(1+\nu)\rho}{E}}$ )

n	Lam and Loy [82]	Bhimaraddi [83]	Shen [84]	Present
1	0.0375	0.0369	0.0371	0.0378
2	0.0367	0.0361	0.0365	0.0365
3	0.0364	0.0357	0.0362	0.0358
4	0.0372	0.0363	0.0370	0.0365

nondimensionalized linear frequencies of composite conical shells achieved from the mentioned method are compared to the results provided by Xiang et al. [59] and Guo et al. [81] in Table 1. The comparison in Table 1 demonstrates that the values obtained from the analytical solution in this study are in excellent agreement with those reported in the cited references.

In order to ensure the accuracy of the presented methodology and solution procedure, Table 2 is also provided for isotropic cylindrical shell, which compares the obtained dimensionless frequency with those available in the literature. As can be observed, the maximum difference between our results and the works of [82–84] is less than 2.4%. The minor discrepancy is related to different theories that have been used in references.

### 3.2. Convergence study

To determine the accuracy and stability of the GDQE method for our problem, the number of grid points (N) are varied until a converged

response is obtained (Fig. 2). The convergence study of grid points is carried out for a cylindrical shell with an auxetic core and without ring support for clamped-clamped boundary conditions. It can be seen that for the first three modes ( $m = 1, m = 2$ , and  $m = 3$ ), the results converge for grid points higher than 7. To increase the accuracy of the GDQE technique, the number of considered grid points is 15.

### 3.3. Influence of different parameters

This section embraces the results of the parametric study on the effect of different parameters involved in the conical shell problem. As mentioned earlier, the conical sandwich shell consists of three layers, with the middle layer being auxetic. The auxetic core, with 6mm thickness, is made of aluminum, with Young's modulus of  $E = 69\text{GPa}$ , shear modulus of  $G = 26\text{GPa}$ , Poisson's ratio of  $\nu = 0.33$ , and density of  $\rho = 2700\text{kg/m}^3$ . The top and bottom layers are also chosen to be made of aluminum with the same material properties. For the cases with ring support, the ring is located in the mid-point of the conical structure, i.e.,  $a = \frac{L}{2}$ . The shell length is  $L = 2m$ , and shell radius is selected to be  $R = \frac{L}{2}$ . The total sandwich shell thickness is considered to be 8mm. As for the auxetic core, the parameters  $\lambda = 3$  and  $\kappa = 0.1$  are considered.

#### 3.3.1. The effect of ring support

Fig. 3 shows the effect of variation of auxetic core interior angle  $\theta$  as well as the semi-vertex angle  $\alpha$  on the first natural frequency of the considered conical shell without ring support. This figure is illustrated for different boundary conditions. It can be observed that decreasing the auxicity of the core (i.e. decreasing  $\theta$ ) results in an increase in the natural frequency of the conical shell (see the right-hand side of the

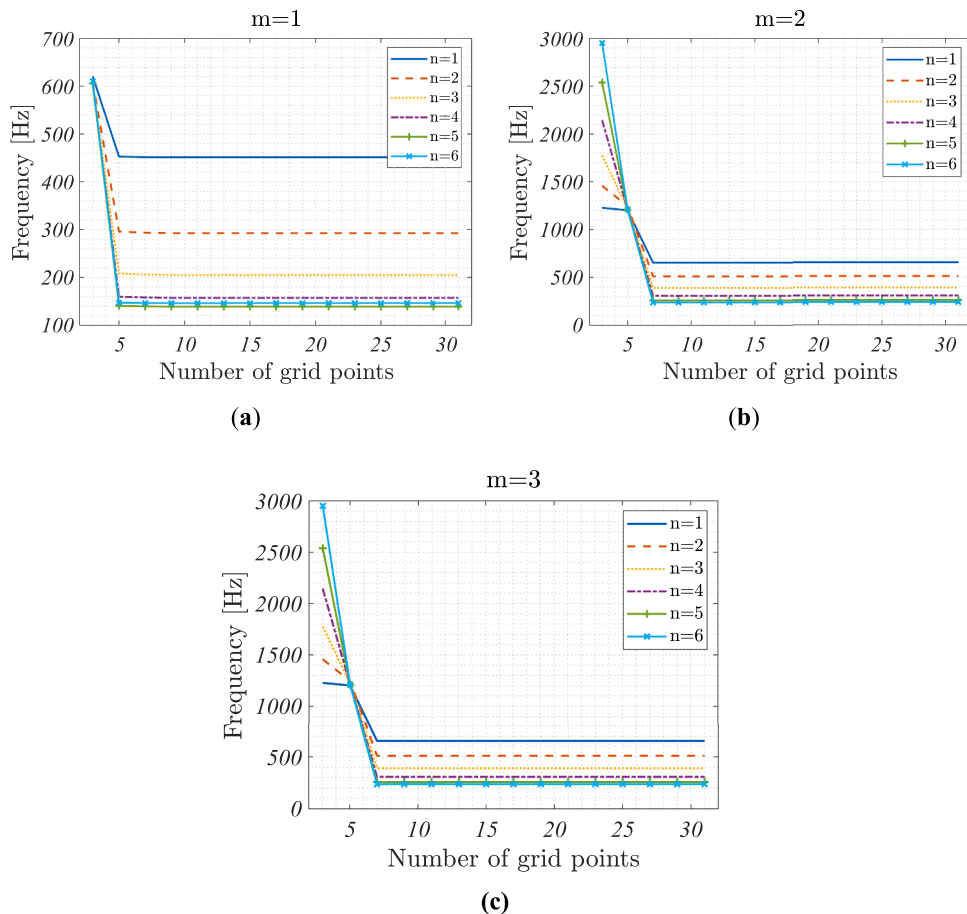


**Fig. 2.** GDQEM convergence study of grid points for a cylindrical shell with auxetic core and without ring support for clamped-clamped boundary condition for mode numbers of (a)  $m = 1$ , (b)  $m = 2$ , and (c)  $m = 3$ .

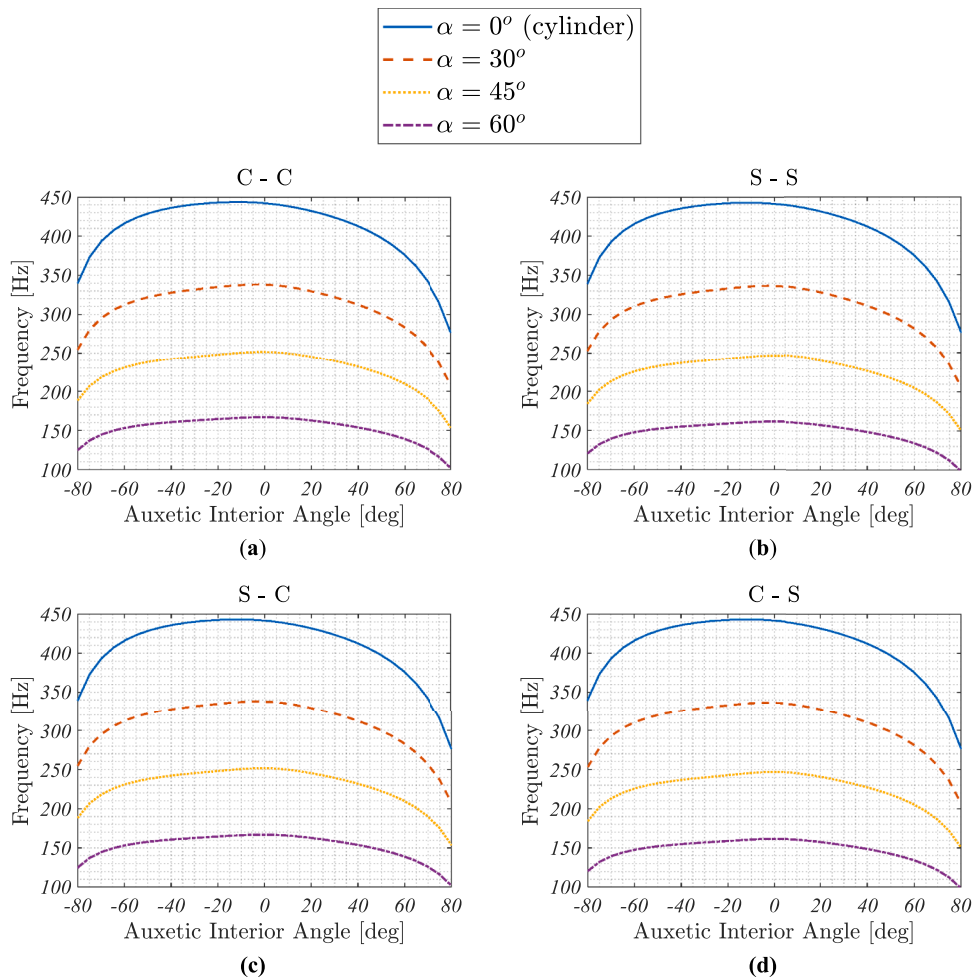


**Fig. 3.** Variation of the first natural frequency for the conical shell without ring support versus the auxetic cell interior angle for different cone angles ( $\alpha$ ) for four types of boundary condition: (a) clamped-clamped, (b) simply supported-simply supported, (c) simply supported-clamped, and (d) clamped-simply supported.

diagrams in Fig. 3). A similar trend can also be observed for decreasing the absolute value of  $\theta$  for a core with a non-auxetic core (see the left-hand side of the diagrams in Fig. 3). Furthermore, regardless of the boundary condition, increasing the cone angle always reduces the shell's natural frequency. The cylindrical geometry, therefore, demonstrates the highest level of natural frequency among all cases. As expected, the fully clamped model (Fig. 3a), possesses the highest frequency because using the C–C boundary condition increases the structural stiffness.

Similar natural frequency graphs are plotted for the cases when ring support is added to the system (Fig. 4). Comparing Figs. 3 and 4 shows that adding a ring to the middle of the structure improves the natural frequency, especially for the cylindrical shape. The trends described in Fig. 3 still hold true in Fig. 4. Fig. 5 plots the natural frequency curves for the cone with and without a ring support to better visualize the effect of adding a ring support. It is evident that adding a ring support enhances the stiffness of the structure.

Tabulated data for all boundary conditions can be found in Table 3. The table is provided to be a comprehensive reference for authors who want to use the presented data for their analysis. It compares the natural frequency of the conical shell for C–C and S–S boundary conditions as well as with and without ring support. In each of the four main cases, the effect of increasing the semi-vertex angles on the longitudinal and circumferential natural frequency levels can be observed as well.

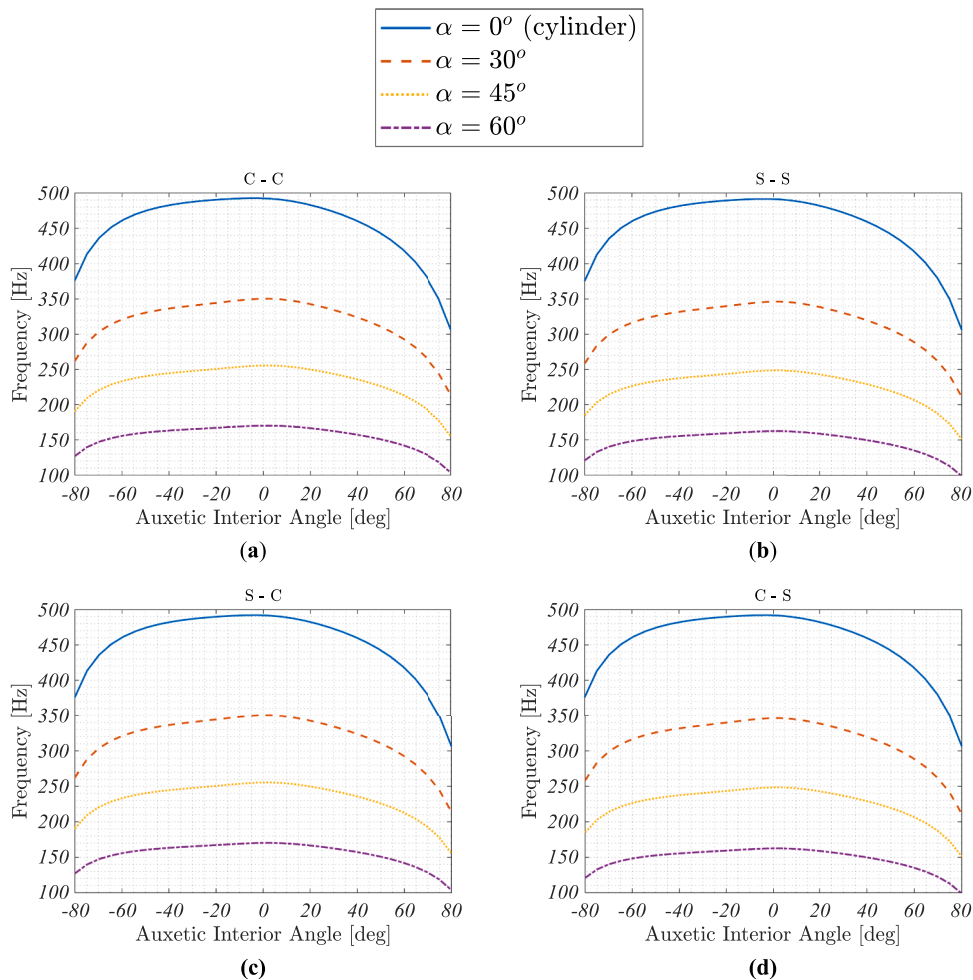
### 3.3.2. The effect of ring positions

Fig. 6 presents the effect of position of stiffened ring on the natural frequency of the conical shell with fully simply supported boundary

conditions for different longitudinal mode shapes. From Fig. 6a, it can be realized that at  $x = 0.1L$  and  $x = 0.9L$ , the presence of the ring support has a negligible effect on the natural frequency. For the first mode, the highest natural frequency is reached at  $x = L/2$ . This is due to the fact that the ring support limits the motion of the middle part of the cylinder, which is supposed to have the highest amplitude of oscillation (see mode 1 in Fig. 7 for the first mode shape of a cylinder without a ring). Due to the same reason, in the second mode, the highest frequency is obtained for  $X = L/4$  and  $x = 3L/4$ . A similar interpretation can be given for higher mode numbers.

In Fig. 6b, the natural frequencies of the conical shell with a  $30^\circ$  cone angle for various positions of the ring support are presented. Similar trends are observed regarding the longitudinal mode shapes of the conical shell. Changing the shell geometry from cylinder to cone results in a shift in the curves' peaks toward the right side (i.e. the side of the cone with higher radius) of the graphs (compare Fig. 6a and b). Therefore, it may be concluded that placing the stiffened ring at positions with higher radii leads to improved natural frequencies. Unlike the cylindrical shell, the relative location of the peak in the case of the cone shell is influenced by some other geometrical/material parameters, such as the shell thickness, cone angle, auxetic interior angle, and material properties.

In Fig. 8, the variation of the natural frequency of the conical shell with respect to the position of two ring supports (both being equally distanced from the two ends of the cone, i.e. at  $x_1 = (\Lambda)L$  and  $x_2 = (1-\Lambda)L$ , where  $0.1 < \Lambda < 0.4$ ) is demonstrated and compared to the case of the cone with one ring support. Fig. 8a presents the special case of the



**Fig. 4.** Variation of the first natural frequency for the conical shell with a ring support versus the auxetic cell interior angle for different cone angles ( $\alpha$ ) for four types of boundary condition: (a) clamped-clamped, (b) simply supported-simply supported, (c) simply supported-clamped, and (d) clamped-simply supported.

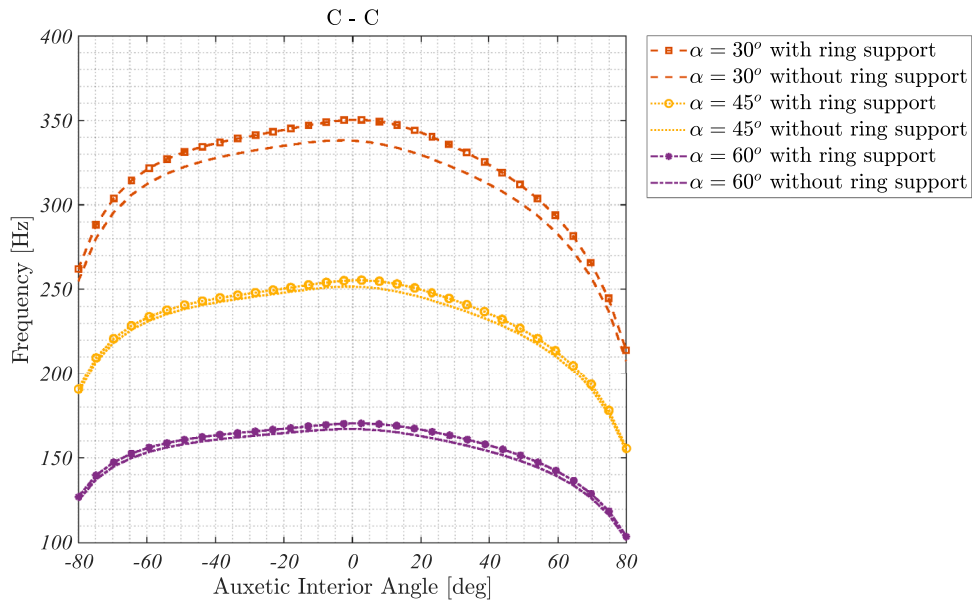


**Fig. 5.** Comparison of the first natural frequency of the conical shell with and without ring support for the clamped-clamped boundary condition.

Table 3

Comparison of the natural frequency of conical shell for C–C and S-S boundary conditions and various semi-vertex angles, while the effect of supportive ring is considered: (a) C–C BC without ring support, (b) S-S BC without ring support, (c) C–C BC with ring support, (d) S-S BC with ring support. In all the cases,  $\theta = -55^\circ$ .

(a) C–C BC without ring support		$n = 1$	$n = 2$	$n = 3$	$n = 4$	$n = 5$	$n = 6$	$n = 7$	$n = 8$	$n = 9$	$n = 10$
$\alpha=0$	$m = 1$	423.96	275.12	192.63	146.33	125.49	126.62	145.47	176.79	216.89	263.83
	$m = 2$	614.14	480.03	365.93	287.83	239.17	214.67	211.45	226.44	255.83	296.14
	$m = 3$	664.13	587.68	498.95	420.63	361.26	322.52	303.96	304.32	321.38	352.33
	$m = 4$	684.94	641.52	581.91	520.45	467.08	427.19	403.26	395.93	404.57	427.62
	$m = 5$	707.58	679.82	640.32	596.47	555.27	522.05	500.26	491.73	497.00	515.58
	$m = 6$	735.52	718.38	692.62	662.97	634.16	610.31	594.61	589.16	595.02	612.43
	$m = 7$	777.37	765.77	748.93	729.71	711.23	696.46	687.92	687.47	696.26	714.84
	$m = 8$	864.08	858.86	850.21	840.45	831.77	826.20	825.54	831.24	844.32	865.42
	$m = 9$	956.43	952.11	945.48	938.58	933.25	931.23	934.00	942.71	958.16	980.85
	$m = 10$	1134.52	1315.60	1586.83	1725.69	1730.92	1738.21	1748.14	1761.21	1777.91	1798.65
$\alpha=30^\circ$	$m = 1$	317.863	231.735	173.597	141.772	132.532	138.722	140.092	131.324	123.212	117.845
	$m = 2$	352.027	325.336	283.050	239.271	204.094	180.933	176.153	178.514	175.935	172.425
	$m = 3$	388.255	365.064	339.440	311.936	285.519	265.407	258.465	267.101	271.421	268.753
	$m = 4$	426.617	406.569	385.281	364.312	344.048	325.604	310.892	304.605	313.972	324.338
	$m = 5$	466.701	450.109	433.188	417.193	402.764	390.720	382.569	381.582	394.069	416.854
	$m = 6$	511.150	499.265	486.903	475.470	465.404	457.041	450.806	447.382	448.524	460.443
	$m = 7$	575.854	568.391	559.822	551.731	545.021	540.318	538.220	539.565	546.029	561.651
	$m = 8$	669.711	668.433	666.736	665.230	664.375	664.503	665.879	668.720	673.219	679.617
	$m = 9$	802.839	801.816	799.938	798.389	797.915	799.128	802.566	808.764	818.381	832.439
	$m = 10$	857.329	1126.743	1290.171	1468.684	1641.958	1646.016	1650.812	1656.568	1663.317	1671.060
$\alpha=60^\circ$	$m = 1$	155.80	127.93	101.91	87.46	84.76	87.75	87.74	85.39	83.53	82.85
	$m = 2$	177.60	164.87	151.08	135.99	123.65	118.04	119.84	122.49	123.95	125.39
	$m = 3$	208.67	196.77	186.09	176.82	170.09	168.11	173.65	183.92	191.66	196.81
	$m = 4$	243.17	235.16	227.22	220.53	215.64	213.12	214.31	221.78	234.86	247.34
	$m = 5$	286.77	282.04	277.67	274.44	272.91	273.68	277.76	287.08	303.73	324.96
	$m = 6$	344.77	343.29	341.90	341.24	341.72	343.63	347.29	353.25	362.77	378.32
	$m = 7$	422.58	422.43	422.81	424.11	426.67	430.77	436.79	445.27	457.26	474.75
	$m = 8$	567.01	567.89	569.44	571.80	575.13	579.54	585.08	591.78	599.69	608.91
	$m = 9$	693.20	694.52	696.83	700.31	705.17	711.65	720.00	730.57	743.79	760.33
	$m = 10$	783.07	977.67	1159.90	1304.06	1457.99	1604.04	1609.79	1616.39	1623.84	1632.06
(b) S-S BC without ring support		$n = 1$	$n = 2$	$n = 3$	$n = 4$	$n = 5$	$n = 6$	$n = 7$	$n = 8$	$n = 9$	$n = 10$
$\alpha=0$	$m = 1$	423.15	273.23	190.05	143.52	122.90	124.56	143.95	175.64	215.95	263.02
	$m = 2$	612.34	477.48	361.91	282.49	233.04	208.44	205.69	221.45	251.57	292.46
	$m = 3$	661.78	583.82	493.33	413.17	352.19	312.38	293.49	294.20	312.04	343.91
	$m = 4$	679.62	635.43	574.22	510.77	455.38	413.79	388.73	381.03	389.98	413.80
	$m = 5$	699.40	670.71	629.60	583.77	540.47	505.28	481.93	472.48	477.52	496.46
	$m = 6$	721.29	703.66	676.80	645.44	614.63	588.79	571.37	564.70	569.98	587.42
	$m = 7$	755.54	743.80	726.27	705.81	685.72	669.23	659.10	657.42	665.50	683.93
	$m = 8$	820.89	815.58	806.94	796.84	787.49	781.08	779.61	784.73	797.60	818.90
	$m = 9$	900.28	896.47	890.95	885.19	880.88	879.74	883.29	892.77	909.08	932.77
	$m = 10$	1134.38	1243.12	1249.79	1256.91	1266.59	1279.51	1296.27	1317.42	1343.47	1374.86
$\alpha=30^\circ$	$m = 1$	315.74	230.16	171.52	139.82	131.43	137.07	134.38	124.04	115.49	109.95
	$m = 2$	340.87	318.22	278.44	234.46	198.75	176.19	172.35	171.09	165.93	161.20
	$m = 3$	378.60	354.14	328.86	302.58	276.72	257.51	253.09	259.34	256.93	252.01
	$m = 4$	416.32	395.53	373.13	351.28	330.48	311.63	297.25	294.78	303.79	308.59
	$m = 5$	456.00	437.65	418.93	401.29	385.53	372.65	364.65	366.42	382.88	397.83
	$m = 6$	499.14	484.49	469.36	455.49	443.40	433.45	426.16	422.74	427.45	447.73
	$m = 7$	550.30	541.58	531.66	522.26	514.33	508.56	505.73	507.09	515.68	538.91
	$m = 8$	617.21	615.35	612.98	610.80	609.34	608.99	610.05	612.84	617.71	625.48
	$m = 9$	737.56	736.67	735.47	734.60	734.72	736.46	740.41	747.22	757.74	773.53
	$m = 10$	856.82	1114.31	1120.85	1124.94	1130.01	1136.18	1143.49	1151.93	1161.45	1172.00
$\alpha=60^\circ$	$m = 1$	150.20	125.53	99.62	85.42	82.98	83.97	81.21	77.59	75.15	74.15
	$m = 2$	169.95	156.27	143.96	129.66	117.75	113.12	113.67	113.62	113.30	113.74
	$m = 3$	200.36	187.52	175.71	165.79	159.21	158.54	164.87	171.51	175.47	178.85
	$m = 4$	233.06	223.50	214.03	206.00	200.28	197.95	201.39	211.56	222.37	230.87
	$m = 5$	270.79	264.32	258.29	253.73	251.33	251.97	257.43	270.40	289.25	305.72
	$m = 6$	317.07	314.87	312.72	311.42	311.47	313.31	317.59	325.72	340.55	362.39
	$m = 7$	382.75	382.69	383.09	384.38	386.96	391.25	397.80	407.64	422.93	447.40
	$m = 8$	498.28	499.41	501.36	504.22	508.12	513.19	519.53	527.28	536.68	548.32
	$m = 9$	150.20	125.53	99.62	85.42	82.98	83.97	81.21	77.59	75.15	74.15
	$m = 10$	169.95	156.27	143.96	129.66	117.75	113.12	113.67	113.62	113.30	113.74
(c) C–C BC with ring support		$n = 1$	$n = 2$	$n = 3$	$n = 4$	$n = 5$	$n = 6$	$n = 7$	$n = 8$	$n = 9$	$n = 10$
$\alpha=0$	$m = 1$	469.51	363.16	307.56	271.10	239.12	214.63	211.41	226.42	255.82	296.14
	$m = 2$	614.13	480.03	365.92	287.80	245.54	231.26	230.32	243.53	269.82	307.17
	$m = 3$	684.72	624.93	555.58	495.86	451.80	423.17	403.26	395.91	404.53	427.56
	$m = 4$	684.95	641.53	581.94	520.49	467.11	427.22	408.82	408.09	420.37	444.79
	$m = 5$	735.66	718.48	692.70	663.03	634.18	610.31	594.60	589.14	595.03	612.47
	$m = 6$	745.20	724.84	696.41	665.97	638.74	618.40	607.06	605.84	615.11	634.83

(continued on next page)

Table 3 (continued)

(c) C–C BC with ring support											
	$n = 1$	$n = 2$	$n = 3$	$n = 4$	$n = 5$	$n = 6$	$n = 7$	$n = 8$	$n = 9$	$n = 10$	
$m = 7$	831.30	825.43	815.84	804.89	794.92	788.13	786.44	791.38	804.05	825.06	
$m = 8$	859.34	849.72	837.80	826.06	816.53	811.12	811.41	818.53	833.21	855.83	
$m = 9$	1058.83	1061.12	1062.19	1064.10	1068.12	1075.24	1086.37	1102.32	1123.73	1151.13	
$m = 10$	1101.86	1236.36	1239.10	1239.52	1241.34	1245.84	1253.93	1266.30	1283.52	1306.05	
$\alpha=30^\circ$	$m = 1$	326.48	272.28	234.08	210.87	196.56	185.96	182.23	187.68	201.47	221.42
	$m = 2$	368.72	342.11	290.59	246.13	219.18	216.15	232.51	259.27	275.28	271.79
	$m = 3$	405.43	365.51	350.82	336.59	322.14	308.53	296.42	286.38	284.60	289.74
	$m = 4$	450.07	445.71	431.29	400.62	371.23	346.80	328.97	320.01	328.15	355.69
	$m = 5$	493.38	468.80	447.82	442.25	438.52	435.55	433.69	433.50	435.72	441.15
	$m = 6$	560.67	551.17	539.18	526.22	514.05	504.51	499.45	500.97	512.10	536.95
	$m = 7$	605.06	603.70	602.56	601.95	602.12	603.19	605.25	608.39	612.75	618.58
	$m = 8$	698.70	695.24	690.74	686.44	683.15	681.44	681.75	684.41	689.71	698.03
	$m = 9$	850.75	905.98	908.17	911.12	915.16	920.50	927.33	935.81	946.12	958.47
	$m = 10$	905.69	1099.19	1125.94	1128.98	1131.92	1135.79	1141.01	1147.90	1156.74	1167.90
$\alpha=60^\circ$	$m = 1$	158.40	144.86	132.04	123.05	117.05	113.74	114.35	119.36	128.59	141.42
	$m = 2$	207.45	188.39	164.91	148.12	142.54	149.95	167.07	186.54	196.44	200.34
	$m = 3$	218.47	208.69	206.79	204.96	203.22	201.87	201.49	203.81	213.10	223.17
	$m = 4$	280.75	272.56	262.47	252.77	245.16	240.81	240.80	247.26	263.64	288.01
	$m = 5$	330.90	330.01	329.61	330.07	331.49	333.95	337.56	342.43	348.70	356.48
	$m = 6$	388.76	386.68	385.28	384.91	386.16	389.70	396.39	407.41	424.51	449.77
	$m = 7$	507.15	508.01	509.55	511.80	514.84	518.71	523.44	529.02	535.50	543.02
	$m = 8$	567.71	568.43	569.98	572.63	576.59	582.04	589.13	598.02	608.93	622.23
	$m = 9$	782.15	831.33	833.93	837.57	842.31	848.22	855.35	863.74	873.46	884.58
	$m = 10$	829.83	974.64	1069.49	1073.44	1077.36	1082.18	1088.10	1095.28	1103.85	1113.99
(d) S-S BC with ring support											
$\alpha=0$	$n = 1$	$n = 2$	$n = 3$	$n = 4$	$n = 5$	$n = 6$	$n = 7$	$n = 8$	$n = 9$	$n = 10$	
$m = 1$	468.43	360.86	304.25	266.77	233.06	208.47	205.73	221.48	251.60	292.49	
$m = 2$	612.34	477.48	361.91	282.50	240.22	225.27	224.18	237.72	264.59	302.56	
$m = 3$	679.02	618.75	547.90	486.31	440.34	409.97	388.73	381.03	389.98	413.79	
$m = 4$	679.62	635.43	574.21	510.77	455.38	413.78	394.31	392.84	405.02	429.86	
$m = 5$	721.81	704.22	677.39	646.08	615.31	589.52	572.15	565.52	570.83	588.28	
$m = 6$	729.28	707.61	678.02	646.13	617.32	595.45	582.85	580.76	589.65	609.48	
$m = 7$	803.58	797.41	787.56	775.99	765.11	757.27	754.58	758.72	770.91	791.81	
$m = 8$	826.30	817.06	805.11	792.92	782.72	776.56	776.16	782.77	797.21	819.89	
$m = 9$	985.67	986.32	987.05	988.76	992.47	999.25	1010.11	1025.98	1047.60	1075.55	
$m = 10$	1042.55	1054.45	1054.94	1056.65	1060.76	1068.19	1079.82	1096.40	1118.53	1146.67	
$\alpha=30^\circ$	$m = 1$	321.886	269.447	230.714	206.900	191.841	180.649	177.107	183.175	197.671	217.589
	$m = 2$	353.326	333.859	286.905	242.150	215.739	214.540	232.491	256.824	258.365	253.703
	$m = 3$	404.814	355.057	335.185	320.695	306.003	291.912	279.163	268.715	271.311	273.085
	$m = 4$	425.508	421.464	416.582	393.828	362.407	336.317	317.913	311.898	328.142	355.138
	$m = 5$	489.330	463.135	430.055	413.670	409.233	405.751	403.476	402.993	405.122	410.873
	$m = 6$	543.896	534.987	522.877	508.973	495.454	484.645	478.935	481.260	495.935	527.478
	$m = 7$	568.676	565.006	562.193	560.671	560.369	561.165	563.040	566.074	570.460	576.853
	$m = 8$	662.272	659.376	655.381	651.243	647.800	645.748	645.661	648.015	653.257	662.069
	$m = 9$	808.500	811.196	813.172	815.956	819.752	824.699	830.916	838.511	847.589	858.269
	$m = 10$	852.158	923.562	926.124	929.294	933.751	939.873	948.016	958.558	971.940	988.740
$\alpha=60^\circ$	$m = 1$	150.776	138.036	125.281	115.895	109.408	105.821	106.411	111.648	121.184	134.076
	$m = 2$	190.179	187.159	162.396	145.138	140.344	149.285	166.018	175.337	177.380	180.058
	$m = 3$	215.497	187.841	185.590	183.503	181.614	180.198	180.391	188.618	199.112	207.014
	$m = 4$	270.778	262.288	251.477	240.592	231.908	227.277	229.016	240.904	262.682	286.017
	$m = 5$	298.766	296.620	295.336	295.340	296.503	298.783	302.275	307.176	313.804	322.595
	$m = 6$	360.710	358.782	357.215	356.609	357.785	361.722	369.688	383.541	405.809	438.046
	$m = 7$	459.752	460.632	462.236	464.588	467.735	471.717	476.572	482.357	489.237	497.844
	$m = 8$	519.826	520.823	522.904	526.179	530.826	537.028	544.977	554.908	567.179	582.491
	$m = 9$	734.048	735.712	738.403	742.137	746.905	752.692	759.468	767.200	775.858	785.430
	$m = 10$	781.736	840.464	844.229	849.295	855.937	864.297	874.521	886.774	901.256	918.226

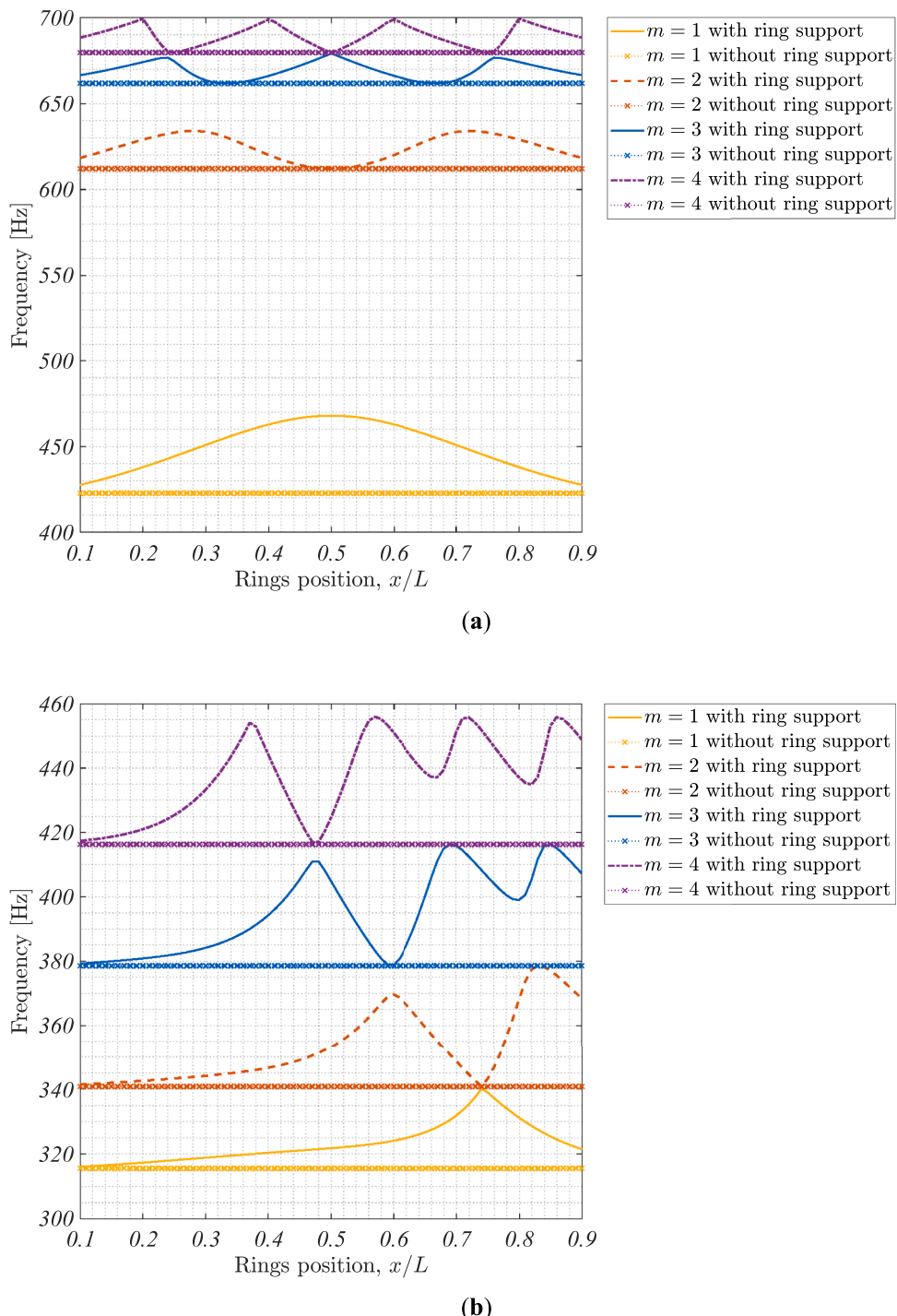
cylindrical shell ( $\alpha = 0$ ). According to this figure, it is apparent that the presence of the second ring can enhance the natural frequency of the system as a result of increase in the stiffness of the entire structure.

Fig. 8b provides the results of the case of the conical shell with  $\alpha = 30^\circ$ . While for the case of one ring, similar trends can be observed for both the cylindrical and cone shells, as for the case of two rings, some obvious differences (in the shape of the curves as well as the location of the peaks) in the results of the cylindrical and cone shells can be observed. The noted differences can be attributed to the effects of the cone angle and non-identical radius of the position where the two rings are placed making the mode shapes asymmetrical.

### 3.3.3. The effect of auxetic cell parameters

The impact of auxetic cell geometrical parameters is investigated in Figs. 9 and 10. The effect of variation of the ratio of horizontal wall length to inclined wall length in the auxetic core, i.e.  $\lambda = e/l$ , on the structure's natural frequency, is demonstrated in Fig. 9. The comparison has been performed for two semi-vertex angles of  $\alpha = 30^\circ$  and  $\alpha = 60^\circ$ . It can be seen that the  $\lambda$  ratio does not affect the frequency level significantly. Nonetheless, it can be stated that higher values of  $\lambda$  are associated with higher natural frequencies. It can also be observed that for positively inclined angles (i.e. for auxetic cores), the effect of  $\lambda$  becomes more distinct.

The effect of cell wall thickness to inclined wall length,  $\kappa$ , on the



**Fig. 6.** The natural frequency of the conical shell with auxetic core versus the ring positions comparing without ring and utilization of one ring support. (a)  $\alpha = 0^\circ$  and (b)  $\alpha = 30^\circ$

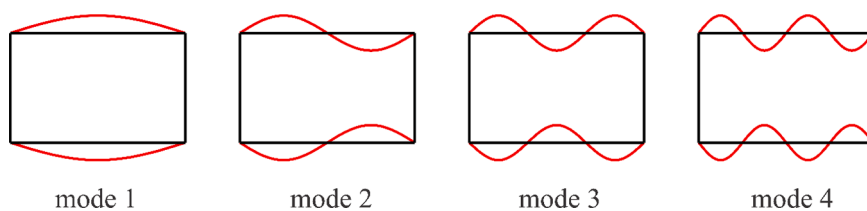


**Fig. 7.** Schematic representation of vibrational mode shapes of a cylinder without ring.

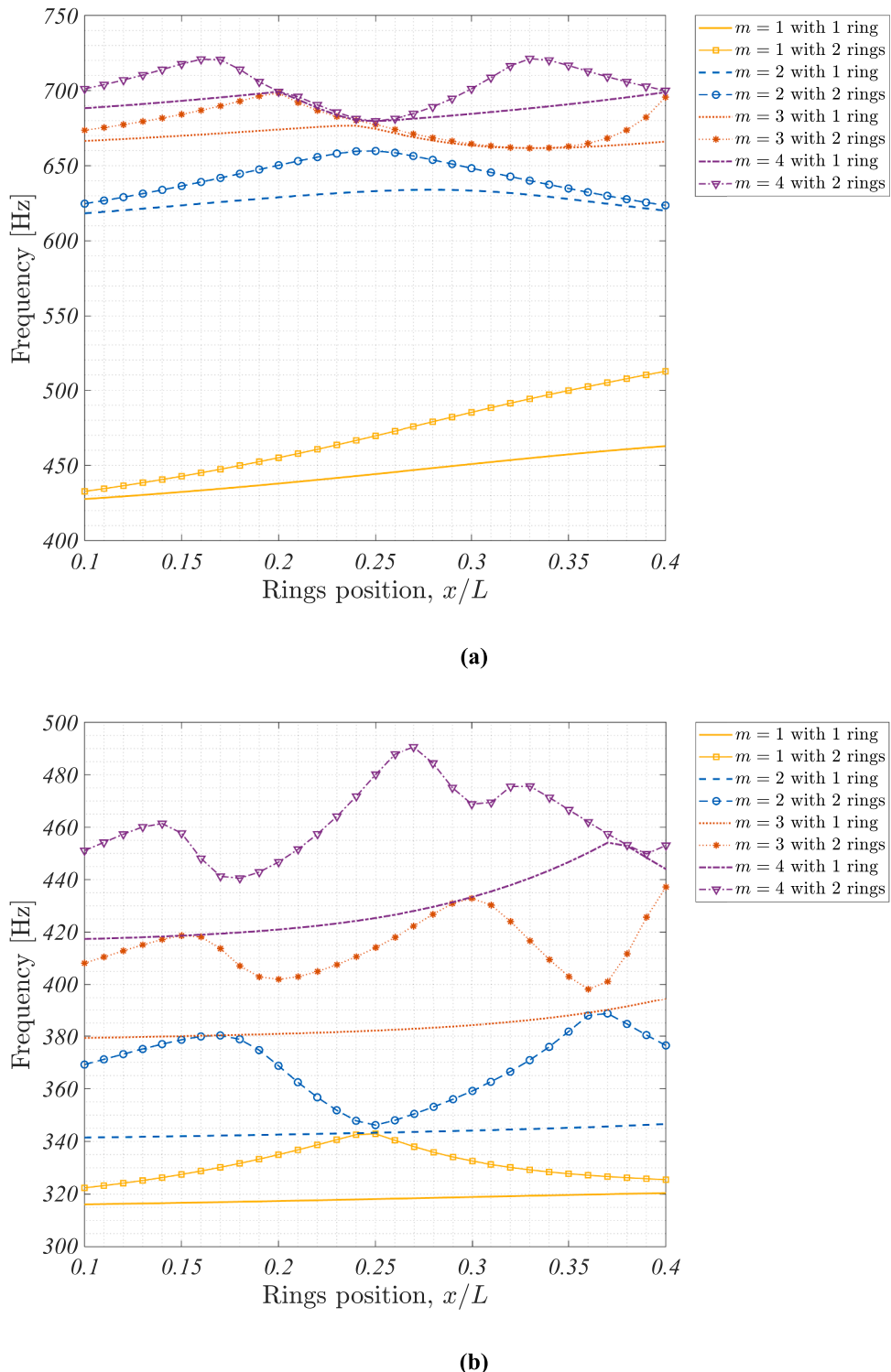


**Fig. 8.** The effect of adding a second ring to (a) cylindrical shell and (b) conical shell (with  $\alpha = 30^\circ$ ) on the natural frequency.

natural frequency of the conical shell is illustrated in Fig. 10. It can be seen that by decreasing the relative thickness  $\kappa$  of the auxetic core, the natural frequency of the system increases. It is known that by increasing either the relative cell wall thickness  $\kappa$  or the value of the cell interior angle  $\theta$ , the density of the core layer increases, while its stiffness increases in one direction and decreases in the other direction (See Fig. A1 in the Appendix). Therefore, it may be concluded that mass change dominates the natural frequency of the structure. This is why increasing  $\kappa$  and/or value of  $\theta$  reduces the natural frequency of the structure (Fig. 10). This is similar to what has been previously reported in

previous work on doubly-curved stiffened sandwich panels with auxetic core [85]. It must be noted that in this work, the auxetic core thickness is considered to be constant. Moreover, in lower cone angles, the effect of changing both the  $\lambda$  and  $\kappa$  ratios become more intense (Fig. 9). As expected, conical shells' frequencies are the highest in fully clamped boundary conditions, as seen in Figs. 9 and 10.

The variation of natural frequency with respect to both the cone angle and the auxetic interior angle is demonstrated in Fig. 11. The goal was to study the effects of the presence of the ring support and boundary condition type on the frequency variations. Comparing the graphs

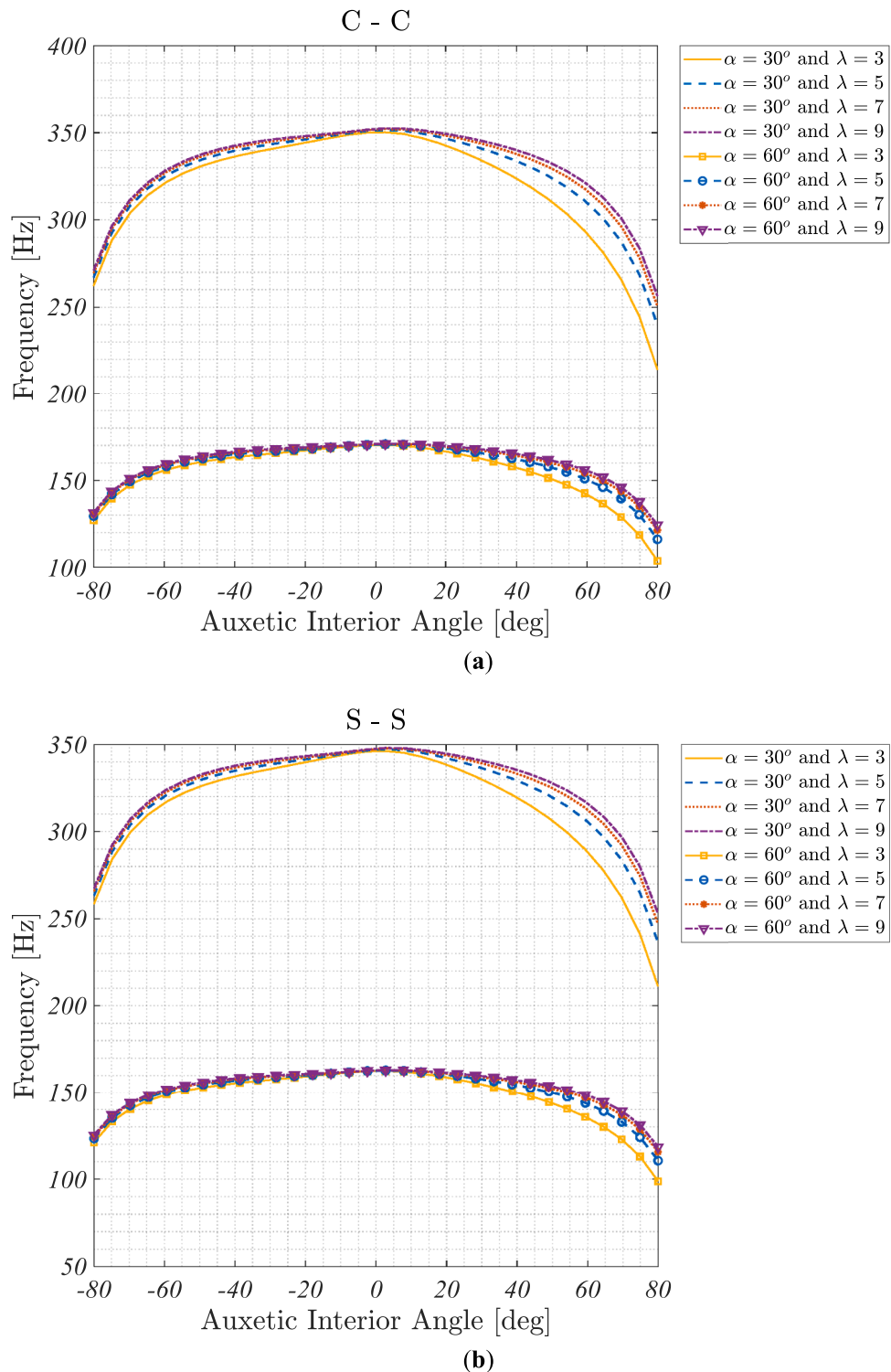


**Fig. 9.** Variation of the first natural frequency of the conical shell with ring support with respect to the auxetic interior angle for four different ratios and for (a) clamped-clamped and (b) simply supported-simply supported boundary conditions.

demonstrates that adding ring support increases the natural frequency regardless of the boundary condition type. This can be attributed to the increase in the overall stiffness of the structure. Moreover, it is evident that increasing both cone and auxetic interior angles decreases the natural frequency, most probably due to a decrease in the stiffness of the shell.

#### 4. Concluding remarks

The main emphasis of this paper was to study the influence of the auxetic core parameters on the vibrational behavior of conical shells. Due to the lack of an analytical study on the impact of negative Poisson's ratio and auxetic parameters on the vibration characteristics of conical shells with/without ring support, this study was performed to investigate impact of these parameters. The influence of the semi-vertex angle,

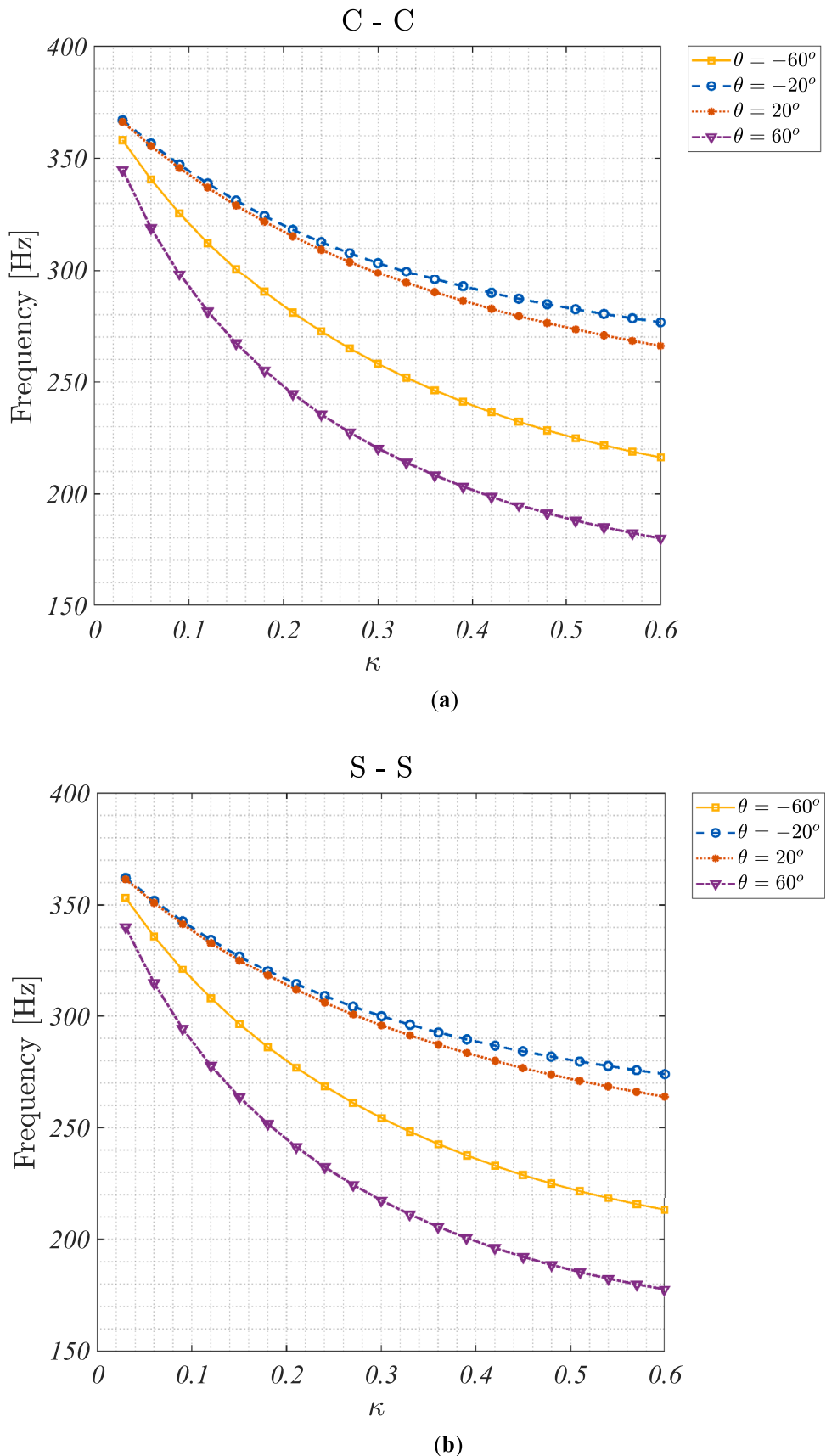


**Fig. 10.** Variation of the first natural frequency for the conical shell with ring support with respect to the auxetic interior angle for four different dimensionless ratios of  $\kappa$ . (a) clamped-clamped, (b) simply supported-simply supported.

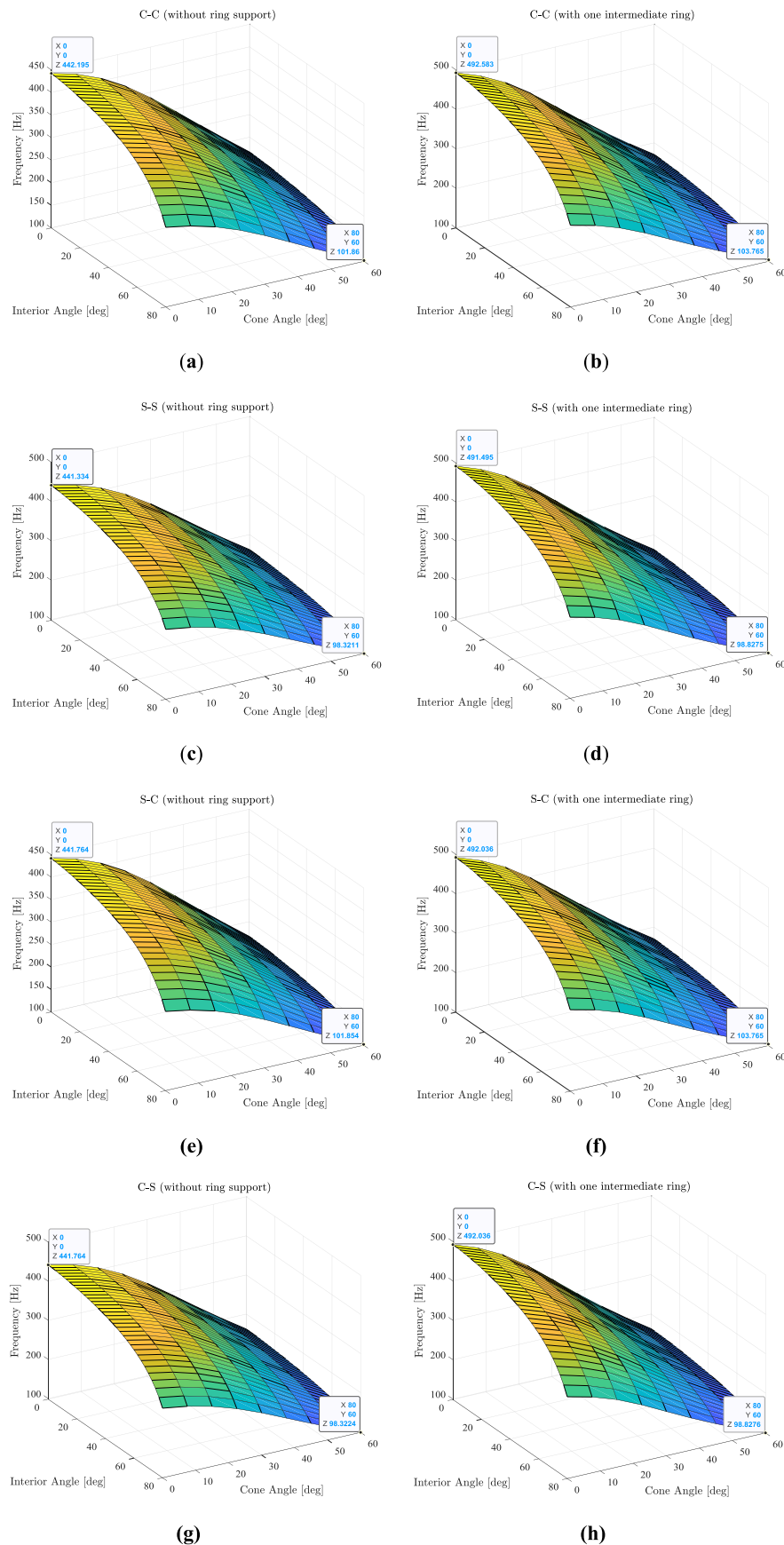


**Fig. 11.** Frequency variation of the conical sandwich shell with and without the ring support in terms of auxetic and cone angles for various boundary conditions. (a) C – C without ring support, (b) C – C with ring support, (c) S – S without ring support, (d) S – S with ring support, (e) S – C without ring support, (f) S – C with ring support, (g) C – S without ring support, (h) C – S with ring support.

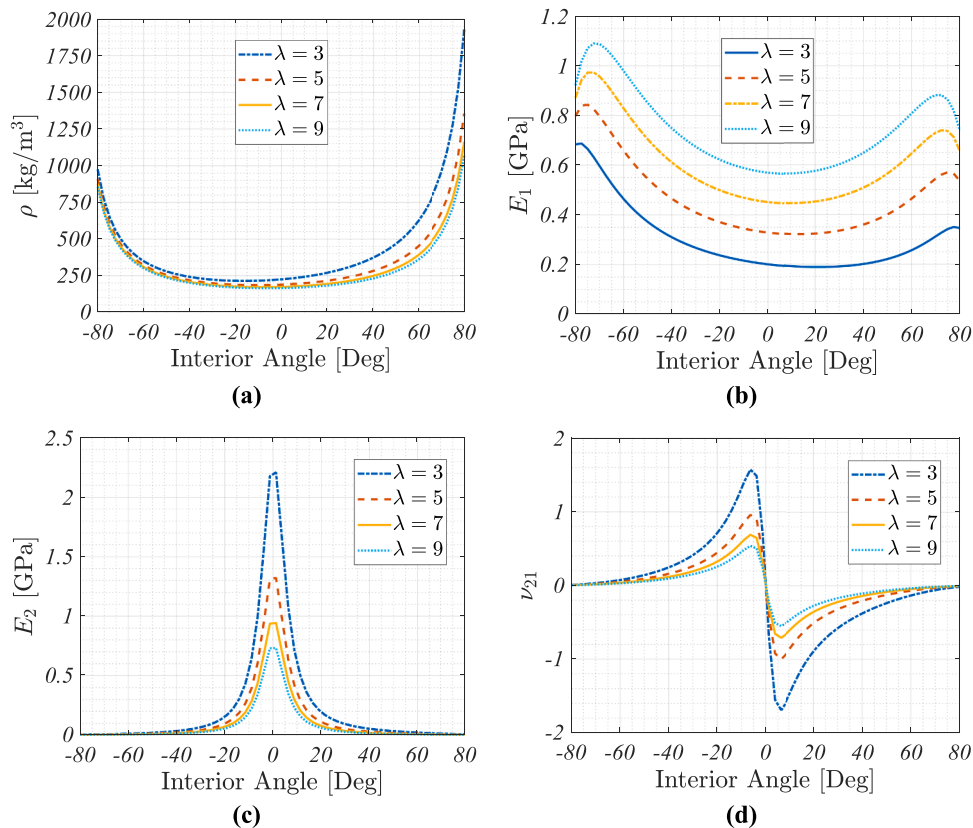


**Fig. A.1.** Variation of the mechanical properties of the auxetic structure with respect to the auxetic interior angle for various rib length ratios: (a) density, (b) Young's modulus  $E_1$ , (c) Young's modulus  $E_2$ , and (d) Poisson ratio of the auxetic core layer.

the auxetic core interior angle, and various boundary conditions was studied as well. The mechanical properties of the auxetic core were extracted from a micromechanical approach and then implemented in the calculations. Afterwards, the FSDT method for shells was utilized, and the governing equations were obtained. Finally, the GDQEM was used to solve the governing equations. The results show that

- introducing an intermediate ring support has a significant impact on natural frequencies of the system. The importance of ring position is found to be highly dependent on longitudinal mode shapes of vibration.
- the impact of ring position on natural frequencies is affected by the semi-vertex angle of the cone, and a shift in frequency peaks can be seen by changing the geometry from cylinder to cone.
- increasing the semi-vertex angle of the cone leads to lower natural frequencies. Consequently, the higher frequencies in all cases belong to the cylinder (i.e. when the semi-vertex angle is zero).
- variation of the auxetic interior angle affects the natural frequencies significantly. By increasing the auxetic interior angle, the natural frequencies decrease.
- other geometrical parameters related to the auxetic core pattern (for instance, the thickness-to-cell wall length ratio) also affect the natural frequencies of the conical sandwich shells. This influence is more distinguishable in lower cone angles.
- the trend of influence of different parameters on the natural frequency of the cones is similar for all boundary conditions. Moreover, stiffer boundary conditions (for instance, clamped-clamped boundary conditions) lead to higher natural frequency values.

#### Declaration of Competing Interest

The authors declare that they have no known competing financial

interests or personal relationships that could have appeared to influence the work reported in this paper.

#### Data availability

Data will be made available on request.

#### Appendix

This section presents the effect of auxetic parameters on the mechanical properties of the auxetic core. Fig. A.1 shows that auxetic interior angle significantly affects the mechanical characteristics of the structure.

#### References

- [1] Wang Z, Zulifqar A, Hu H. Auxetic composites in aerospace engineering. In: Rana S, Figueiro R, editors. Advanced composite materials for aerospace engineering. Woodhead Publishing; 2016. p. 213–40.
- [2] Baughman RH. Auxetic materials: avoiding the shrink. *Nature* 2003;425(6959): 667.
- [3] Dirrenberger J, Forest S, Jeulin D. Effective elastic properties of auxetic microstructures: anisotropy and structural applications. *Int J Mech Mater Des* 2013;9(1):21–33.
- [4] Ghavidelina N, Bodaghi M, Hedayati R. Idealized 3D auxetic mechanical metamaterial: an analytical, numerical, and experimental study. *Mater (Basel)* 2021;14(4):993.
- [5] Kolken HMA, et al. Mechanical performance of auxetic meta-biomaterials. *J Mech Behav Biomed Mater* 2020;104:103658.
- [6] Kolken HMA, et al. Mechanisms of fatigue crack initiation and propagation in auxetic meta-biomaterials. *Acta Biomater* 2022;138:398–409.
- [7] Kolken HMA, et al. Fatigue performance of auxetic meta-biomaterials. *Acta Biomater* 2021;126:511–23.
- [8] Ghavidelina N, Bodaghi M, Hedayati R. Femur auxetic meta-implants with tuned micromotion distribution. *Materials (Basel)* 2021;14(1):114.

- [9] Plewa J, Płońska M, Feliksik K. An experimental study of auxetic tubular structures. *Materials (Basel)* 2022;15. <https://doi.org/10.3390/ma15155245>.
- [10] Assidi M, Ganghoffer J-F. Composites with auxetic inclusions showing both an auxetic behavior and enhancement of their mechanical properties. *Compos Struct* 2012;94(8):2373–82.
- [11] Kochmann DM, Venturini GN. Homogenized mechanical properties of auxetic composite materials in finite-strain elasticity. *Smart Mater Struct* 2013;22(8):084004.
- [12] Wang S, et al. Design and modeling of a novel three dimensional auxetic reentrant honeycomb structure for energy absorption. *Compos Struct* 2022;280:114882.
- [13] Madke RR, Chowdhury R. Anti-impact behavior of auxetic sandwich structure with braided face sheets and 3D re-entrant cores. *Compos Struct* 2020;236:111838.
- [14] Jafari Nedoushan R, et al. Novel triangular auxetic honeycombs with enhanced stiffness. *Compos Struct* 2021;277:114605.
- [15] Jiang L, Gu B, Hu H. Auxetic composite made with multilayer orthogonal structural reinforcement. *Compos Struct* 2016;135:23–9.
- [16] Li P, et al. Improved explicit co-simulation methods incorporating relaxation techniques. *Arch Appl Mech* 2020;90(1):17–46.
- [17] Duc ND, et al. New approach to study nonlinear dynamic response and vibration of sandwich composite cylindrical panels with auxetic honeycomb core layer. *Aerosp Sci Technol* 2017;70:396–404.
- [18] Lim T-C. Buckling and Vibration of Circular Auxetic Plates. *J Eng Mater Technol* 2014;136(2).
- [19] Parhi, J.D. and T. Roy, *Chaotic vibration analysis of auxetic nanocomposite structures*. *J Vib Control*. 0(0): p. 10775463221123206.
- [20] Jiang L, Hu H. Low-velocity impact response of multilayer orthogonal structural composite with auxetic effect. *Compos Struct* 2017;169:62–8.
- [21] Dabbagh A, Ebrahimi F. Postbuckling analysis of meta-nanocomposite beams by considering the CNTs' agglomeration. *Eur Phys J Plus* 2021;136(11):1168.
- [22] Ebrahimi F, Nopour R, Dabbagh A. Smart laminates with an auxetic ply rested on visco-Pasternak medium: active control of the system's oscillation. *Eng Comput* 2021.
- [23] Hajmohammad MH, et al. A new numerical approach and visco-refined zigzag theory for blast analysis of auxetic honeycomb plates integrated by multiphase nanocomposite facesheets in hygrothermal environment. *Eng Comput* 2019;35(4):1141–57.
- [24] Behravan Rad A. Static analysis of non-uniform 2D functionally graded auxetic-porous circular plates interacting with the gradient elastic foundations involving friction force. *Aerosp Sci Technol* 2018;76:315–39.
- [25] Li C, Shen H-S, Yang J. Design and nonlinear dynamics of FG curved sandwich beams with self-adapted auxetic 3D double-V meta-lattice core. *Eng Struct* 2022;272:115023.
- [26] Li C, Shen H-S, Yang J. Low-velocity impact response of cylindrical sandwich shells with auxetic 3D double-V meta-lattice core and FG GRC facesheets. *Ocean Eng* 2022;262:112299.
- [27] Li C, Yang J, Shen H-S. Postbuckling of pressure-loaded auxetic sandwich cylindrical shells with FG-GRC facesheets and 3D double-V meta-lattice core. *Thin-Wall Struct* 2022;177:109440.
- [28] Li C, et al. Large amplitude vibration of sandwich plates with functionally graded auxetic 3D lattice core. *Int J Mech Sci* 2020;174:105472.
- [29] Shen H-S, Li C, Reddy JN. Large amplitude vibration of FG-CNTRC laminated cylindrical shells with negative Poisson's ratio. *Comput Methods Appl Mech Eng* 2020;360:112727.
- [30] Li C, Shen H-S, Wang H. Nonlinear vibration of sandwich beams with functionally graded negative Poisson's ratio Honeycomb core. *Int J Struct Stab Dyn* 2019;19(03):1950034.
- [31] Tornabene F, Fantuzzi N, Bacciochi M. Linear static behavior of damaged laminated composite plates and shells. *Materials (Basel)* 2017;10(7):811.
- [32] Javani M, Kiani Y, Eslami MR. Application of generalized differential quadrature element method to free vibration of FG-GPLRC T-shaped plates. *Eng Struct* 2021;242:112510.
- [33] Bagheri H, Kiani Y, Eslami MR. Free vibration of joined conical-cylindrical-conical shells. *Acta Mech* 2018;229(7):2751–64.
- [34] De Rosa MA, et al. Nonlocal vibration analysis of a nonuniform carbon nanotube with elastic constraints and an attached mass. *Materials (Basel)* 2021;14(13):3445.
- [35] Cao Z, et al. Novel semi-analytical solutions for the transient behaviors of functionally graded material plates in the thermal environment. *Materials (Basel)* 2019;12(24):4084.
- [36] Talezadehli A. Free vibration analysis of perforated composite cylindrical shell and panel using multi-domain generalized differential quadrature (GDQ) method. *Compos Struct* 2022;287:115337.
- [37] Li H, et al. Vibration analysis of porous metal foam truncated conical shells with general boundary conditions using GDQ. *Compos Struct* 2021;269:114036.
- [38] Abediokhchi J, Shakouri M, Kouchakzadeh MA. Bending analysis of moderately thick functionally graded conical panels with various boundary conditions using GDQ method. *Compos Struct* 2013;103:68–74.
- [39] Tornabene F, Liverani A, Caligiana G. Laminated composite rectangular and annular plates: a GDQ solution for static analysis with a posteriori shear and normal stress recovery. *Compos Part B: Eng* 2012;43(4):1847–72.
- [40] Andakhshideh A, Maleki S, Aghdam MM. Non-linear bending analysis of laminated sector plates using Generalized Differential Quadrature. *Compos Struct* 2010;92(9):2258–64.
- [41] Zamani M, Fallah A, Aghdam MM. Free vibration analysis of moderately thick trapezoidal symmetrically laminated plates with various combinations of boundary conditions. *Eur J Mech - A/Solids* 2012;36:204–12.
- [42] Xiang Y, et al. Exact solutions for vibration of cylindrical shells with intermediate ring supports. *Int J Mech Sci* 2002;44(9):1907–24.
- [43] Hou S, et al. The free vibration analysis of carbon nanotubes-reinforced deep conical shells with an intermediate ring support under various boundary conditions. *Engineering Structures* 2022;263:114291.
- [44] Bagheri H, Kiani Y, Eslami MR. Free vibration of conical shells with intermediate ring support. *Aerosp Sci Technol* 2017;69:321–32.
- [45] Dong Y, et al. TE-GDQE implementation to investigate the vibration of FG composite conical shells considering a frequency controller solid ring. *Eng Anal Bound Elem* 2022;138:95–107.
- [46] Eipakchi H, Nasrekanli FM. Axisymmetric analysis of auxetic composite cylindrical shells with honeycomb core layer and variable thickness subjected to combined axial and non-uniform radial pressures. *Mech Adv Mater Struct* 2022;29(12):1798–812.
- [47] Van Quyen N, et al. Nonlinear forced vibration of sandwich cylindrical panel with negative Poisson's ratio auxetic honeycombs core and CNTRC face sheets. *Thin-Walled Struct* 2021;162:107571.
- [48] Duc ND, et al. Mechanical stability of eccentrically stiffened auxetic truncated conical sandwich shells surrounded by elastic foundations. *Mech Compos Mater* 2022;58(3):365–82.
- [49] Kamarian S, et al. Free vibration analysis of conical shells reinforced with agglomerated Carbon Nanotubes. *Int J Mech Sci* 2016;108–109:157–65.
- [50] Li F-M, Kishimoto K, Huang W-H. The calculations of natural frequencies and forced vibration responses of conical shell using the Rayleigh–Ritz method. *Mech Res Commun* 2009;36(5):595–602.
- [51] Sobhani E, Masoodi AR, Ahmadi-Pari AR. Vibration of FG-CNT and FG-GNP sandwich composite coupled Conical-Cylindrical-Conical shell. *Compos Struct* 2021;273:114281.
- [52] Nopour R, et al. Nonlinear forced vibrations of three-phase nanocomposite shells considering matrix rheological behavior and nano-fiber waviness. *Eng Comput* 2022.
- [53] Farkas J, Jármai K, Farkas J, Jármai K, editors. *8 - Welded Stiffened cylindrical and conical shells, in design and optimization of metal structures* 2008:167–223.
- [54] Maheesh V. Nonlinear free vibration of multifunctional sandwich plates with auxetic core and magneto-electro-elastic facesheets of different micro-topological textures: FE approach. *Mech Adv Mater Struct* 2021:1–22.
- [55] Hamdia KM, et al. Stochastic analysis of the fracture toughness of polymeric nanoparticle composites using polynomial chaos expansions. *Int J Fract* 2017;206(2):215–27.
- [56] Vu-Bac N, et al. Uncertainty quantification for multiscale modeling of polymer nanocomposites with correlated parameters. *Composit Part B: Eng* 2015;68:446–64.
- [57] Vu-Bac N, et al. A software framework for probabilistic sensitivity analysis for computationally expensive models. *Adv Eng Softw* 2016;100:19–31.
- [58] Hamdia KM, et al. Sensitivity and uncertainty analysis for flexoelectric nanostructures. *Comput Method Appl Mech Eng* 2018;337:95–109.
- [59] Xiang X, et al. A numerical solution for vibration analysis of composite laminated conical, cylindrical shell and annular plate structures. *Compos Struct* 2014;111:20–30.
- [60] Bodaghi M, Shakeri M, Aghdam MM. Thermo-mechanical behavior of shape adaptive composite plates with surface-bonded shape memory alloy ribbons. *Compos Struct* 2015;119:115–33.
- [61] Aghdam MM, Shahmansouri N, Bigdeli K. Bending analysis of moderately thick functionally graded conical panels. *Compos Struct* 2011;93(5):1376–84.
- [62] Reddy JN. Mechanics of laminated composite plates and shells: theory and analysis. CRC press; 2003.
- [63] Shu C. Free vibration analysis of composite laminated conical shells by generalized differential quadrature. *J Sound Vib* 1996;194(4):587–604.
- [64] Viswanathan KK, et al. Vibration analysis of cross-ply laminated truncated conical shells using a spline method. *J Eng Math* 2012;76(1):139–56.
- [65] Kalkhorani VA, Aghdam MM. Novel predictor-corrector formulations for solving nonlinear initial value problems. In: Dai L, Jazar RN, editors. *Nonlinear approaches in engineering application: design engineering problems*. Cham: Springer International Publishing; 2022. p. 55–67.
- [66] Kabir H, Aghdam MM. A generalized 2D Bézier-based solution for stress analysis of notched epoxy resin plates reinforced with graphene nanoplatelets. *Thin-Walled Struct* 2021;169:108484.
- [67] Ebrahimi F, Nopour R, Dabbagh A. Effects of polymer's viscoelastic properties and curved shape of the CNTs on the dynamic response of hybrid nanocomposite beams. *Waves Rand Compl Med* 2022;1–18.
- [68] Ebrahimi F, Nopour R, Dabbagh A. Effect of viscoelastic properties of polymer and wavy shape of the CNTs on the vibrational behaviors of CNT/glass fiber/polymer plates. *Eng Comput* 2022;38(5):4113–26.
- [69] Mohammadi N, Asadi H, Aghdam MM. An efficient solver for fully coupled solution of interaction between incompressible fluid flow and nanocomposite truncated conical shells. *Comput Method Appl Mech Eng* 2019;351:478–500.
- [70] Anitescu C, et al. Artificial neural network methods for the solution of second order boundary value problems. *Comput Mater Continua* 2019;59(1):345–59.
- [71] Guo H, Zhuang X, Rabczuk T. A deep collocation method for the bending analysis of Kirchhoff Plate. *Comput Mater Continua* 2019;59(2):433–56.
- [72] Samaniego E, et al. An energy approach to the solution of partial differential equations in computational mechanics via machine learning: concepts, implementation and applications. *Comput Method Appl Mech Eng* 2020;362:112790.

- [73] Nguyen-Thanh VM, et al. Parametric deep energy approach for elasticity accounting for strain gradient effects. *Comput Methods Appl Mech Eng* 2021;386:114096.
- [74] Fallah AA, Mohammadi M. Physics-informed neural network for bending and free vibration analysis of three-dimensional functionally graded porous beam resting on elastic foundation. *Eng Comput* 2023.
- [75] Niknam H, Fallah A, Aghdam MM. Nonlinear bending of functionally graded tapered beams subjected to thermal and mechanical loading. *Int J Non Linear Mech* 2014;65:141–7.
- [76] Jahromi HN, Aghdam MM, Fallah A. Free vibration analysis of Mindlin plates partially resting on Pasternak foundation. *Int J Mech Sci* 2013;75:1–7.
- [77] Chen C-N. A generalized differential quadrature element method. *Comput Method Appl Mech Eng* 2000;188(1):553–66.
- [78] Shafiei N, Mousavi A, Ghadiri M. Vibration behavior of a rotating non-uniform FG microbeam based on the modified couple stress theory and GDQEM. *Compos Struct* 2016;149:157–69.
- [79] Sahmani S, Aghdam MM, Bahrami M. On the free vibration characteristics of postbuckled third-order shear deformable FGM nanobeams including surface effects. *Compos Struct* 2015;121:377–85.
- [80] Sahmani S, et al. Surface effects on the nonlinear forced vibration response of third-order shear deformable nanobeams. *Compos Struct* 2014;118:149–58.
- [81] Guo S, Hu P, Li S. Free vibration analysis of composite conical shells using Walsh series method. *Mater Res Expt* 2021;8(7):075303.
- [82] Lam KY, Loy CT. Effects of boundary conditions on frequencies of a multi-layered cylindrical shell. *J Sound Vib* 1995;188(3):363–84.
- [83] Bhimaraddi A. A higher order theory for free vibration analysis of circular cylindrical shells. *Int J Solid Struct* 1984;20(7):623–30.
- [84] Shen H-S. Nonlinear vibration of shear deformable FGM cylindrical shells surrounded by an elastic medium. *Compos Struct* 2012;94(3):1144–54.
- [85] Pham H-A, et al. Free vibration analysis and optimization of doubly-curved stiffened sandwich shells with functionally graded skins and auxetic honeycomb core layer. *Thin-Walled Struct* 2022;179:109571.